# The annual cycle of the West African monsoon in a two-dimensional model: mechanisms of the rain-band migration

Philippe Peyrillé, P. Lafore, Aaron Anthony Boone

QUARTERLY JOURNAL OF THE ROYAL METEOROLOGICAL SOCIETY
RMetS Royal Meteorological Society

# The annual cycle of the West African Monsoon in a two-dimensional model: Mechanisms of the rain band migration



| | |
|---|---|
| Journal: | *QJRMS* |
| Manuscript ID | QJ-15-0216.R1 |
| Wiley - Manuscript type: | Research Article |
| Date Submitted by the Author: | n/a |
| Complete List of Authors: | Peyrille, Philippe; CNRM Meteo-France & CNRS,<br>Lafore, Jean-Philippe; CNRM, GMME/MOANA;<br>Boone, Aaron; CNRM Meteo-France & CNRS, |
| Keywords: | monsoon, seasonal cycle, rain band location, water recycling, shallow meridional circulation, ITCZ, idealized modelling |
| | |

# The annual cycle of the West African Monsoon in a two-dimensional model: Mechanisms of the rain band migration

P. Peyrillé[1], J.-P. Lafore and A. Boone

CNRM-GAME, Météo-France and CNRS, Toulouse, France

ABSTRACT

The processes that drive the annual cycle of the West African Monsoon (WAM) are analysed using an idealized meridional-vertical numerical model that includes moist physics. Using the work by Peyrillé and Lafore (2007) as a starting point, the framework has beenis adapted to studying the annual cycle. A suitable forcing methodology for temperature and humidity has been is derived which allowsing the two-dimensional (2D) model to reproduce the main features of the WAM.

A budget analysis of the simulated temperature and humidity variables leads to a picture of the InterTropical Convergence Zone (ITCZ) seasonal displacement, for which the moistening on the northern side of the ITCZ is a key. It is due to the near surface moisture advection by the monsoon flow to the north of the ITCZ, in addition to the turbulent fluxes and shallow convection which transport moisture to the top of the planetary boundary layer. On a larger scale, the warming of the Saharan Heat Low by turbulence and radiation and the cooling/moistening within the ITCZ by convective downdrafts reinforces the monsoon flow. Inertial instability is also at play favouring the acceleration of the monsoon flow and the associated humidification. These mechanisms seem to be at play during the whole seasonal cycle, which is seen as a steady translation of these structures.

Sensitivity experiments show the importance of the low level processes such as downdrafts, horizontal advection and water recycling. Although advection is the 1st order

1 *Corresponding author address*: P. Peyrillé, CNRM-GAME, Météo-France, 42 Av. G. Coriolis, 31057 Toulouse, France
E-Mail: philippe. peyrille@meteo.fr

process, the water recycling appears as a key element by directly modulating the intensity of rainfall and by allowing the convective downdrafts to feed back onto the WAM.

## 1. Introduction

The West African monsoon (WAM) and the associated rainfall is a climatological system of major economic and social importance that is characterized by a large spatio-temporal variability (Janicot *et al.,* 2008). In particular, the WAM shows a distinctive annual cycle that is at first order, described by the meridional migration of the associated rain band from an equatorial oceanic location in winter to a continental location at around 10°N in summer. A detailed description of the annual cycle has been given by Thorncroft *et al.* (2011), who considered the water vapour transport over West Africa. The WAM annual cycle can be characterized by four key phases that are intimately tied to the variations of sea surface temperature (SST) in the Tropical Atlantic (Okumara and Xie, 1997; Zheng *et al.* 1999 ) and to the Saharan heat Low (Sultan and Janicot 2003, Thorncroft *et al.* 2011, Ramel *et al.* 2006). An oceanic phase takes place from November to mid-April when the rainfall peak is around 2-3°N. It is followed by a coastal phase from mid-April to the end of June when the InterTropical Convergence Zone (ITCZ), defined here as the location of the maximum rainfall, is positioned along the southern coastal region. A transitional phase occurs between June and mid-July when the rainfall peak decreases over the coast and moves northward towards the Sahel. The last (Sahelian) phase is when the rainfall peak is over the Sahel with intensities on the order of 8-10 $mm.day^{-1}$.

Despite this simple description, the annual cycle remains a challenge to model and predict. Vizy and Cook (2006) showed that a first order feature of the annual cycle, such as the meridional displacement of the rain band, is poorly handled by CMIP3 climate models. Roehrig *et al.* (2013) evaluated the current climate simulations of the WAM in CMIP5 models. They found that the monsoons simulated by climate models (GCMs) exhibit systematic biases and a large dispersion, particularly in terms of the summer rainfall spatial

and temporal distributions**.** The GCMs place the summer peak rainfall either several degrees too far to the north or to the south, and the associated rainfall intensities range from half to twice the amount observed. They underscored the SST warm bias in the Gulf of Guinea, the misrepresentation of the diurnal cycle of convection over land, and the large dispersion in the representation of the intra-seasonal variability and the cloud radiative effect. Overall this study highlighted the need to obtain a better understanding of the basic drivers of the annual cycle of the WAM.

Fundamentally, the monsoon results from the interplay between the warm/dry continental low-pressure system called the Saharan heat low (SHL) and the cool/moist ocean that feeds the monsoon flow with moisture. Both phenomena are characterized by a strong annual cycle that modulates the location and intensity of the rain band. This simple view, based mainly on the precipitation, is limited by the strong link between the different types of heating (dry over the Sahara and moist in the ITCZ; Thorncroft and Blackburn 1999), the resulting circulation, and the surface features that ultimately shape the monsoon. During the annual cycle, the deep overturning circulation associated with the ITCZ takes moist static energy from the ocean to the continent, with ascent close to the latitude of the maximum low-level moist static energy. In contrast, the SHL dry Shallow Meridional Circulation (SMC, Zhang et al. 2008, Hagos and Zhang 2009) is confined between the surface and approximately 700 hPa, with ascent close to the Inter-Tropical Discontinuity (ITD) and the maximum surface temperature, which enforces a moisture flux convergence maximum to occur northward of the rain band (Thorncroft el al. 2011; Hagos and Cook 2007; Hurley and Boos 2013). The SHL has also been found to impact the variability of rainfall over the Sahel in both CMIP5 climate models (Biasutti et al. 2009) and in reanalysis (Hurley and Boos 2013, Roehrig et al. 2011), pointing out the key role of this region in shaping the rain band.

In the quasi-equilibrium framework, the WAM can be described in terms of subcloud moist static energy (MSE) – or alternatively by the subcloud equivalent potential temperature $\theta e$ – and dry static energy (Eltahir and Gong 1996; Hurley and Boos 2013). Processes affecting those meridional profiles, north or south of the rain band will thus impact the monsoon circulation that in turns may modulate the subcloud layer $\theta e$ (Eltahir and Gong 1996; Peyrillé and Lafore 2007; Hurley and Boos 2013). The Tropical Atlantic ocean affects the intensity and location of rainfall (Ward 1998; Zheng *et al*. 1999; Peyrillé *et al.* 2007) and the phasing of coastal rainfall (Thorncroft *et al.* 2011), but continental processes are important too. The surface albedo and its meridional gradient are among the most recognized factors that limit the northward migration of the monsoon (Charney 1975; Chou and Neelin 2003; Ramel 2006). Other continental characteristics, such as those related to the vegetation or the soil moisture values and their respective gradients, also modulate rainfall and the meridional gradient of $\theta e$ (Zheng and Eltahir 1996; Xue and Shukla 1998; Zou 2001; Philippon *et al.* 2005; Koster 2004; Chou and Neelin 2004). However, the role of some key processes linked to the continental water budget such as surface evapotranspiration, drainage or runoff have not been clearly established in terms of the WAM annual cycle. It may be linked to the large spread of the representation of these processes in current land surface models (Boone *et al.* 2009) which has limited the understanding of their impact over West Africa.

While viewing the WAM on the basis of $\theta e$ is indeed informative, it does not allow an understanding of the evolution of the annual cycle since the evolution of the $\theta e$ meridional profile, the circulation, diabatic processes and dry dynamics are intimately coupled and interact during the seasonal cycle. In terms of dry dynamics, Tomas and Webster (1997) - TW97 hereinafter - showed that the release of inertial instability can help understand the mean location of the rainband over West Africa. This region is characterised by a zero

absolute vorticity (η) line crossing the equator owing to the advection of negative absolute vorticity from the southern hemisphere by the monsoon flow. Although the release of inertial instability is difficult to detect using observations, evidences of inertial instability suggest it plays a key role in the African monsoon onset (Cook 2014, Hagos and Cook 2007) and interannual variability (Nicholson and Webster 2006). Hagos and Cook (2007) analysed the interaction between the dry and moist dynamics using a numerical model. They found that the monsoon jump arises following two steps; there is a strengthening of the SHL that they associated with the albedo profile, and second, because of a supply of moisture at low levels that helps convection to develop. Following the arguments of TW97 and Tomas et al. (1999), they suggest that the resulting pressure gradient favours the release of inertial instability and it initiates the monsoon onset.Thorncroft *et al.* (2011) confirmed this view considering the water vapour transport over the WAM during the annual cycle. They noted that a peak of moisture flux convergence occurs about 8° poleward of the rainfall peak, mainly driven by the SHL and the associated SMC. However, no clear process analysis of the complete water budget was given since only the water vapour transport was considered. Cook (2014) also noted the decrease of rainfall at the coast is associated with the relase of inertial instability in the region.

The processes driving the annual cycle are numerous and the annual cycle can be seen as their combination at different time scales, ranging from the diurnal up to the seasonal. This complexity limits the accuracy of GCMs, making the source of biases difficult to identify, and it reflects our limited understanding of the WAM annual cycle. As a contribution in that direction, the main goal of the present paper is to better identify the role of some of the key mechanisms that drive the annual cycle, notably those linked to the continental water cycle, the SMC, the ITCZ heating, and the meridional gradient of heating, and then to quantify their relative contributions within the mean annual cycle.

With this objective in mind, we consider an idealized numerical framework in order to reduce the complexity of the system. Previous studies have analyzed the WAM with simplified models using a quasi-equilibrium hypothesis (Chou and Neelin 2004) or by taking advantage of the strong zonal symmetry over West Africa (Eltahir and Gong 1996, Zheng *et al.* 1999, Peyrillé *et al.* 2007). Zheng *et al.* (1999) investigated the role of SST during the annual cycle and found a delayed response of Sahelian precipitation to a SST anomaly. The model did not however represent the cloud-radiation feedback or any diurnal cycle. Peyrillé and Lafore (2007: PL07 hereafter) studied a steady state monsoon using a model with a complete physical package. They needed to include both a temperature and a moisture large-scale forcing, mainly consisting of zonal advection terms. They showed that this forcing can be a key in terms of blocking the monsoon migration.. Although some recent studies have shown that eddies (Schneider and Bordoni, 2008; Bordoni and Schneider, 2010) or intraseasonal modes of variability (Maloney and Shama; 2008, Poan et al. 2014) can significantly modulate the mean meridional circulation, we assume that the two dimensional framework retains enough physics, which are typical of the WAM, to make it a useful analytic tool. The model in this study takes advantage of the complete physical package of the numerical model from PL07 to investigate the key processes of the annual cycle. So far, the model has been used for the study of a steady monsoon regime, therfore the first objective of this paper is to assess the ability of the 2D model to reproduce the main features of the WAM annual cycle. This study focuses on the relative importance of the SMC, the continental moist processes and the atmospheric diabatic processes that may affect the MSE profile.

The numerical model and the methodology developed to study the annual cycle are described in section 2. Section 3 provides a description of the control simulation of the annual cycle and the sensitivity to the forcing, while the rain band displacement is investigated owing

to budget computation in section 4. Section 5 describes the sensitivity of the annual cycle to some of the key processes. The last section discuss the results and conclusions.

## 2. Methodology and numerical model

*a) Data*

The NCEP2 reanalysis (Kalnay *et al.* 1996) at a 1.5° resolution is used in this study to evaluate whether the 2D model is able to reproduce the basic features of the WAM and to derive the external forcing of the 2D model. Reanalysis products exhibit different characteristics in the West African region, especially in terms of mean annual cycle of the ITCZ (location and intensity of summer rainfall mainly) and of meridional-vertical circulation (Zhang *et al.* 2008, Meynadier *et al.* 2010). Therefore the same reference simulations were performed with the ERA40 (Uppala *et al.* 2005) and ERAInterim (Dee *et al.* 2011) reanalyses (not shown). It was verified that the major results and mechanisms discussed in this paper are not sensitive to which reanalysis is used to derive the forcing, thus results obtained with NCEP2 are presented herein for brevity.

The Global Precipitation Climatology Project (GPCP) daily precipitation (Huffman *et al.* 2001) is also used to estimate the ability of the 2D model to reproduce the main features of the WAM annual cycle.

*b) Description of the model*

The 2D latitude-height model developed in PL07 is based on the Meso-NH non-hydrostatic model (Lafore *et al.* 1998, Stein *et al.* 1999). It is described in detail in Peyrillé *et al.* (2007) and PL07, so that here only its main characteristics are reviewed. The model domain spans the latitudinal band between 30°S and 40°N at a relatively low horizontal resolution (150km) and it extends up to 22 km using 22 vertical levels with finer resolution in

the lowest levels (6 in the first 1.5 km). After verification that basic results are not too sensitive to vertical and horizontal resolutions, we adopted this rather crude resolution to perform simulations over several years. The model domain represents a longitudinally averaged latitude-height cross-section between 10°E and 10°W. The surface is considered to be land between 5°N and 35°N in order to mimic the African continent surrounded by ocean conditions. A flat continent without orography is also considered for the sake of simplicity.

The representation of radiative transfer usesthe Fouquart and Bonnel (1980) scheme for solar radiation and using the Rapid Radiative Transfer Model (RRTM) of Mlawer *et al.* (1997) for the longwave fluxes. We use the Kain-Frish-Bechtold scheme for deep convection (Bechtold *et al.* 2001) which includes downdrafts and rainfall evaporation. Turbulence is parameterized following Cuxart *et al.* (2001) while thermals and shallow non precipitating convection are represented using the Pergaud *et al.* (2011) scheme. The aerosol radiative effect is included in the model by prescribing the aerosol climatology from Tegen et al. (2003). The continent is coupled to the atmosphere through prognostic equations for temperature and humidity using the ISBA land surface model (Noilhan and Planton 1989) within the SURFEX platform (Masson *et al.* 2013).

Over the ocean, the SST is prescribed using the Reynolds estimate from the Extended Reconstructed Sea Surface Temperature (ERSST, Reynolds *et al.* 2002) dataset. [10°W-10°E] Mean monthly values are prescribed for the Atlantic, and the average [10°E-20°E] for the Mediterranean Sea, north of 35°N is used. These monthly profiles are linearly interpolated in time in order to prescribe the SST annual cycle. The continental surface characteristics (albedo, roughness, root depth) are obtained after a zonal averaging is applied to the Ecoclimap land cover database (Masson et al. 2003). As mentioned in the introduction, the model includes an external forcing that represents the effect of zonal inhomogeneities on temperature and humidity. In order to simulate several annual cycles, the forcing

methodology used by PL07 (used to study a steady regime over one month) has been modified, and it is described in the following subsection.

*c) Modifications of the atmospheric forcing*

PL07 introduced a large-scale forcing term in their idealized 2D simulations of the monsoon in order to account for the missing advection terms in a 2D framework for temperature and water vapour, which has been derived for July 2000 using the ERA-40 reanalysis. In a first step, this approach was used with the NCEP2 reanalysis in order to perform a 2D simulation of the entire annual cycle, but the penetration of the monsoon was too far northward with a rain band at 20°N in the summer which was too intense. In order to understand this failure, we revisit the assumptions made to derive these large-scale advective forcing terms.

1) LIMITS OF THE 2D FRAMEWORK

Figure 1a shows tests which explored the accuracy of the first assumption (considering the WAM as a zonally symmetric feature) by showing the zonal divergence term (color) superposed on the zonal wind as diagnosed from NCEP2 reanalyses. Examination of the zonal wind field allows the identification of some key features associated with the WAM in the summer: *i.e.* the low level westerlies (monsoon layer) topped by the African Easterly jet (AEJ) at 600 hPa, in the upper troposphere the Tropical Easterly Jet (TEJ) which spans the equatorial latitudes with two subtropical westerly jets (STJ) on its northern and southern sides. The zonal divergence, du/dx is the zonal gradient of the mean zonal wind. It displays a broad convergence in the upper troposphere, especially in the 20S°-30°N latitudinal band. There is divergence in the lower layers over the ocean between the surface and 850 hPa. This large-scale feature can be thought as the fingerprint of zonal interactions of the WAM region

with the rest of the tropics which is consistent with the mean subsiding motion of 0.01 $Pa.s^{-1}$ that takes place over West Africa (Fig. 1b). Since the vertical velocity obtained when integrating only the zonal contribution du/dx to the horizontal divergence (red curve) compares fairly well with the domain averaged vertical velocity, this implies that the mean subsiding motion that prevails over West Africa and the Tropical Atlantic is mainly due to the zonal interactions of the WAM with the rest of the Tropics. This subsiding large-scale motion could be considered as relatively weak, so that to a first order, the zonal symmetry could be considered as a good approximation for the WAM. Nevertheless, this assumption could have major impacts for long-lasting simulations attempted here. First, the associated warming and drying in the free atmosphere cannot be neglected. Second, the mass conservation assumed in the 2D framework implies a modification of the circulation in the latitudinal-vertical profile as compared with the reanalysis. This is illustrated by comparing the NCEP2 mean meridional wind $V$ (Fig. 1c) in JAS, with $V_{nd,}$ the non-divergent meridional wind in the meridional vertical plane (Fig. 1d) computed for the same mean vertical cross-section [10°E-10°W]. The latter term is obtained by integrating the vertical divergence term $\partial(\omega)/\partial p$, meridionaly and by imposing the same boundary conditions as in the 2D model, i.e. v=0 on the southern and northern boundaries (i.e. after imposing the [10°W-10°E]-[30°S-40°N] averaged pressure velocity to be zero). This integration yields the meridional wind that is required to satisfy mass conservation in the vertical-meridional plane assuming that the 2D model is able to reproduce (at best) the observed vertical velocity.

The observed and derived meridional winds both display the same general structures in the lower levels with converging winds in the low levels towards 10°N and diverging, poleward winds at 200 hPa (Fig. 1c,d). The difference is that using the mass continuity in the 2D meridional-vertical plane to compute $V_{nd}$ leads to a dramatic overestimation of the intensity (+3 m.s-1) and thickness of the monsoon flow over the whole range of southerlies

between 1000 hPa and 850 hPa. Between 20°N and 30°N, the northeasterly continental trade wind known as the Harmattan is underestimated, which favours a global northward drift of the monsoon. Between 200 and 100 hPa there is a negative bias, leading to a relatively weak northern branch of the Hadley cell and too strong a southern branch associated with overly intense northerlies.

The assumption of 2D flow geometry therefore leads to a northward drift of the low level winds and an overly-intense direct deep circulation. The impact of the wall lateral boundary conditions used by the 2D model has been tested by varying the domain size. Although spurious vertical circulations are generated close to these north and south wall boundaries, they have a relatively weak impact on the simulated WAM circulation.

## 2) METHOD TO COMPUTE THE LARGE-SCALE FORCING

Together with the imperfections of the parameterizations of the 2D model, it is concluded that the above limitations of the 2D framework are the main reasons for the failures of the simulation of the monsoon annual cycle when the PL07 methodology is used. To overcome this limitation, a simple 2-step procedure has been adopted to derive the large-scale forcing terms. First, a 3-year simulation is done in which the temperature and humidity fields are relaxed towards the two-dimensional NCEP2 zonal-monthly means with a short time-scale $\tau_I$ of 3 days. The relaxation tendencies are stored at a daily frequency during the last year in order to compute monthly averaged tendencies which are then prescribed as pure external forcing in a second set of simulations. This methodology offers the advantage of applying the ad-hoc correction to the model and only those second simulations will be analyzed. A 10-day relaxation is still applied in the second set of experiments for temperature and humidity with a time-scale which permits the model to avoid a slow drift of the monsoon system. It is an order

of magnitude smaller than the forcing and may be viewed as a way to account for the equilibrium between the WAM region and the global circulation.

Figure 2 displays the resulting forcing in JAS. A warming/drying structure (1 $K.d^{-1}$ / 0.5 $g\ .kg^{-1}.d^{-1}$) occurs in the free troposphere which is consistent with the subsiding motion shown in Fig. 1b. In the low levels, a warming/drying occurs just over the oceanic surface while a cooling/moistening affects the north of the SHL, around 25°-35°N, with magnitudes of $-2K.d^{-1}$ and $1g.kg^{-1}.d^{-1}$. On the southern flank of the SHL, a warming/drying structure in the same range ($1K.d^{-1}$ / $-1kg^{-1}.d^{-1}$) occurs. The forcing is discussed in greater detail in section 3.b where the same structure are found for each season with an increased magnitude during spring and summer (Fig. 5).This new forcing has many similarities with the advective forcing directly derived from NCEP2 with the PL07 approach, except for the warming/drying structures in the free atmosphere and on the southern edge of the SHL that were not found here (see PL07, Fig. 2). This later feature helps maintain the SHL against meridional advection by the monsoon flow. It can be interpreted as the correction by the new forcing of the excessive cooling/moistening by meridional advection due to the overestimation of the monsoon intensity and depth in the 2D framework (Fig. 1d).

*d) Experimental design and set of simulations*

Starting from a dry initial state at rest for the atmosphere and at the wilting point water content for the soil, the model is integrated 3 years with a 3-day relaxation to let the soil reservoirs reach an equilibrium, and to compute the atmospheric forcing from the last year (see the previous subsection). Starting from there, the model is then integrated 3 more years using the new forcing, which is considered to be a period which is long enough to obtain a statistically-equilibrated annual cycle (longer experiments show little inter-annual variability).

Note that no inter-annual variations of SST or large scale forcing are applied in such a configuration which keeps the model application simple.

Table 1 summaries the sensitivity experiments that have been performed in order to document and explore the impact of the forcing and the role played by some key processes on the ITCZ displacement. The relaxation timescale, $\tau_1$, which is used to determine the forcing, is varied from 1 to 30 days. Then the impact of the corresponding forcing on the WAM annual cycle simulation is tested. A set of experiments which explore the model sensitivity to the $\tau_2$ timescale has also been conducted to determine its optimal value (10 days, not shown). The last set of sensitivity experiments explored the role of the main processes that are expected to contribute to the Sahel moistening, which focus on the water recycling, the convective downdrafts and the advection by the SMC. The results of these are analyzed in detail in section 5.

## 3. Simulation of the annual cycle

*a) General view of the annual cycle*

In this section, the ability of the 2D model to represent the main features of the WAM annual cycle is presented. Figure 3 shows the evolution of GPCP rainfall compared to the 2D model simulated values with and without forcing. Without forcing, the annual cycle of rainfall is far from the observations, with an excessive northward shift and large rainfall intensities (20 $mm.d^{-1}$) associated with a steady band of precipitation along the Guinean Coast (Fig. 3a,b). The forcing prevents this bias, with a good timing and reasonable intensities of the coastal and Sahelian regimes (Fig. 3a,c). The winter regime is not reproduced as well, however, with rainfall located over land too early. However, one should be aware that even in a simple configuration, such as the 2D model, the obtained rainfall lies in the range of solutions obtained with state-of-the-art GCMs (Roehrig *et al*. 2013).

Figure 4 compares the 2D model with NCEP2 for some key parameters relevant to the WAM. The meridional vertical distribution of potential temperature is well reproduced with the meridional gradient between the ocean ($\theta$ ~300K) and the SHL ($\theta$ > 315K) although it is slightly overestimated (Fig. 4a,b). The streamfunction, $\psi$, in the 2D vertical plane depicts the direct circulation associated with the deep convective overturning well (Fig. 4c,d). The stronger vertical gradient of $\psi$ in the low levels shows an overestimation of the depth and intensity of the monsoon flow that can be viewed as a limitation of the 2D framework which was explained in section 2.c. The vertical structure is somewhat bimodal (shallow and deep circulations) in the 2D model compared to NCEP2, but it is known to have a stronger shallow circulation on average compared to other reanalyses (Zhang *et al.* 2008).

The evolution of the mean $\theta$ in the low levels reveals the seasonal migration of the SHL, from 10°N in Spring to up to ~20°N in summer (Fig. 4c). The migration is well captured in the 2D model (Fig. 2d), but it is overestimated (25°N in summer) in relation with an SHL which is too strong (315K). The overall movement of the maximum area of PW is well represented by the 2D model, with a good progression of the PW maximum from the ocean in winter to the continent in Spring (Fig. 4e, f). The main default of the model is a moisture excess throughout the year with values reaching 65 mm against 60 mm in NCEP2. In winter, a PW maximum is found around the equator in the 2D model in agreement with NCEP2, while rainfall peaks further to the north, which is possibly linked to the 2D framework limitations and to the physical parameterizations caveats.

The 2D model successfully simulates the gross features of the monsoon and their intensity, which are the ITCZ, the SHL, and the meridional-vertical circulation. Therefore it is expected that the present idealized 2D model can correctly reproduce the main interactions between the principal actors during the seasonal migration of the monsoon.

*b) Sensitivity to the forcing*

Figure 5 shows the rainfall and the forcing obtained with different relaxation timescales. The meridional-vertical structure of the forcing terms during the summer has already been shown (Fig. 2) and discussed in section 2.c for a 3-day relaxation timescale ($\tau_1$). The major features in the low levels (0-2 km layer, Fig. 5e) are the warming/drying over ocean (~0.5/-0.5 $K.d^{-1}$), a stronger warming/drying over the continent south of 20N (max ~1/-3 $K.d^{-1}$), and a reverse structure (cooling/moistening ~-1.5/0.5 $K.d^{-1}$) to the North in the SHL. A similar structure is diagnosed in spring (Fig. 5c) and winter (Fig. 5a) with a similar magnitude, but it is shifted southward at ~16°N and 5°N in spring and winter, respectively, in agreement with the monsoon seasonal migration. The sensitivity of forcing terms to the relaxation timescale ($\tau_1$) is similar for all seasons. They retain the same structures, especially for moisture, with an increased magnitude and a more southerly location with reduced $\tau_1$.

Regarding the precipitation, a stronger relaxation leads to lower rainfall during all of the seasons together with a southward shift of its northern margin (Fig. 5 right). In summer and spring, $\tau_1$=1 day leads to precipitation which is too weak, while $\tau_1$= 5 days causes the rain band go to far to the north (Fig. 5d,f). The winter regime shows the same tendency except the 2D model fails to locate the rain band over the ocean regardless of $\tau_1$, confirming that the winter regime is not well handled by such a simple framework.

The sensitivity study shows the structures of the forcing are conserved using different $\tau_1$ and that the forcing prevents the northward migration of the rain band. The use of a 3-day timescale allows a reasonable fit to the observed rainfall in spring and summer, which justifies the use of this value to determine the forcing.

## 4. Analysis of the rain band displacement

*a) Analysis of the heat and moisture budgets*

In order to analyze the ITCZ displacement, the structure of the budgets of potential temperature $\theta$ and water vapour $q$ contributing to the MSE budget (which are considered as key variables of the WAM system) are examined. They are directly computed during the 2D model integration with the following equation set:

$$\frac{\partial \theta}{\partial t} = -v\frac{\partial \theta}{\partial y} - w\frac{\partial \theta}{\partial z} + \frac{\partial \theta}{\partial t}^{frc} + \frac{\partial \theta}{\partial t}^{conv} + \frac{\partial \theta}{\partial t}^{turb} + \frac{\partial \theta}{\partial t}^{rad} \quad (1)$$

$$\frac{\partial q}{\partial t} = -v\frac{\partial q}{\partial y} - w\frac{\partial q}{\partial z} + \frac{\partial q}{\partial t}^{frc} + \frac{\partial q}{\partial t}^{conv} + \frac{\partial q}{\partial t}^{turb} \quad (2)$$

where the *r.h.s.* terms represent the meridional and vertical advection, the forcing, the tendency associated with deep convection (including resolved clouds) and turbulent transfers (including shallow non-precipitating convection), respectively. The last extra-term of the heat budget (Eq. 1) corresponds to the radiative source. They are averaged over one month and analyzed for 3 key periods of the annual cycle: April, June and August in Figs. 6, 7 and 8, respectively. The $\eta$=0 contour is also overlayed in order to depict the unstable inertial zone.

Figure 6 shows the $\theta$ (left) and $q$ (right) budgets together with $\psi$ for April, a period during which the SHL is reinforced. A log-representation is adopted for the vertical axis in order to zoom in on the low-level structures which play a key role within the WAM. The streamfunction shows the monsoon circulation driven by thermal contrast between the ocean and SHL. The monsoon layer is 1.5 km deep and penetrates over the continent up to the ITD located at ~15°N in April, as in NCEP2 (black line in Fig. 4). The forced vertical ascent at the ITD up to 3km, and the return flow of the SMC are clearly identified by the streamfunction, whereas ascent in the ITCZ in the free atmosphere exhibits a double structure with some convection over the Gulf of Guinea at the equator and over the continent up to 10°N, which is coherent with the observed and simulated precipitation evolution (Fig. 3a, c and Fig. 6c).

Between 0 and 2 km the η=0 contour shows an inertially unstable region from the equator to 5-8°N. Consistent with the results of TW97, the main rain band corresponding to the monsoon is located at 8-10°N, just north of the η=0 contour (Fig. 6c).

At this time of the year there is a net warming tendency by the heat budget north of 15°N in the SHL region (Fig. 6a). The major contribution to this heating is turbulence (Fig. 6e), up to 3 km, which is reduced by the advection in the low levels and the forcing throughout the planetary boundary layer (PBL: Fig. 6g,i). South of the ITD over the continent, the heat budget is balanced. The equilibrium in the low levels (below 3 km) results from a complex balance between horizontal advection, turbulence and convection. Below 1.5 km, the advection by the monsoon flow cools the atmosphere (Fig. 6g) while deep convection reinforces this cooling below 1 km (Fig. 6c), due to rain evaporation which feeds cold pools. This cooling of the monsoon layer is balanced mainly by the PBL heating (Fig. 6e,i) and for a weak part, by the forcing (Fig. 6i). In the SMC return flow (1.5-3 km layer), the heat budget is balanced between the heating by deep convection (Fig. 6c) and cooling by detrainment of shallow convection above the PBL (Fig. 6e).

The moisture budget (Fig. 6 right column) indicates a weak evolution in April, except a net moistening at the head of the monsoon just south the ITD (Fig. 6b). The northward transport by the moist monsoon layer causes a strong moistening in this region up to 1 km (Fig. 6h), which is partly compensated by the turbulent transport in the PBL, which dries the lowest levels and moistens the overlying layers (Fig. 6f). The forcing term reduces the total net moistening (Fig. 6j), acting against the overestimated meridional advection in the 2D framework. The sloped layer of moistening over the continent corresponds to the detrainment of shallow convection at the top of the PBL whose depth increases northward towards drier conditions (Fig. 6f). This moistening is compensated by the drying associated with the deep

convection, illustrating the strong coupling between shallow and deep convection, and other processes.

In summary, in April the circulation is dominated by the SHL through a shallow circulation, which is strengthened by the increasing differential heating between the ocean and the SHL due to the turbulent heat transport. The moisture is increased north of the ITCZ by the joint action of advection by the monsoon flow and turbulent transfer. Following TW97, the release of inertial instability is also at play with an increased advection of negative $\eta$ by the monsoon flow that favours wind convergence and a meridional wind maximum north of the $\eta=0$ contour (not shown). Thus it likely strengthens the humidification associated with the base state monsoon flow between 10°N and 15°N (Fig. 6b).When the ITCZ arrives over the Sahel (June) and reaches its mature stage (August), the budgets present many similarities with the pre-monsoon period in April. The major change is the northward shift of all structures corresponding to the seasonal march of the WAM (Fig. 7,8). In June, the ITD reaches ~18°N and the rain band extends from the coast to ~15°N, whereas in August, the ITD is at ~20°N, the coastal rain band is weaker and the main rain band is between 8 and 18°N (Fig. 7c,d). The associated deep convective overturning (see streamlines) is stronger than in April. The net heating differs with the period under considerations. In June, a net warming is found in the SHL as in April, but a net cooling occurs to the south below 3 km (Fig. 7a). This cooling/warming dipole allows the monsoon penetration and is characteristic of the onset period. This cooling region results from stronger rain evaporation (Fig. 7c) and horizontal advection (Fig. 7g) that cannot be fully compensated by the turbulence (Fig. 7e), in contrast to what occurs in April. The forcing reduces this dipole and thus the monsoon penetration, but it remains a less significant term. Two months later, the total temperature tendency vanishes and even reverses which is consistent with the maximum penetration

reached by the WAM in August and the start of its retreat (Fig. 7b), so that all terms of the heat budget begin to decrease. The zero absolute vorticity line shows a deeper inertially unstable region between the equator and 8°N for June and August than in April (Fig. 6c,7c,7d) with deep convection and downdraft cooling well delimited by the η=0 contour.

Concerning the moisture budget (Fig. 8), the moisture increases at the northern leading edge of the monsoon layer in June, as in April, whereas a drying is diagnosed in August. A remarkable feature is the convective drying associated with the ITCZ over the continent following the monsoon penetration between June and August (Fig 8c,d). The structure of the advection in low levels can be characterized as: in the monsoon layer below 1.5 km, drying on the southern flank of the ITCZ and a strong moistening to the north, up to the ITD are seen. The opposite structure is observed above 1.5 km in the mid-level branch of the SMC (Fig. 8g, h). The combination of turbulence and shallow convection (Fig. 8e, f) balances the advection term and the deep convective drying except at the head of the monsoon in June. It should be noticed that the Q1 and Q2 terms estimated by Poan et al (2014) from ERA-I (see their Fig. 2) present many similarities with or Fig. 7-8cdef, which gives added confidence concerning the previous analysis of the processes.

*b) Seasonal evolution of the heat and moisture budgets over Sahel*

The main structures of the budgets are conserved from month to month consistent with the WAM displacement. A more continuous view is given here with the time evolution of these budgets at 15°N (Fig. 9).

First there is a rainless period from January to April (Fig. 9j) corresponding to convection being inhibited by the subsidence in the free troposphere (Fig. 9c,d). At this time, the latitude 15°N corresponds to the core of the SHL and shows the typical balance previously analyzed (Fig.6). The 0-3km layer is heated by turbulence in the lowest levels while advection

(subsidence and SMC) in conjunction with radiation warm the 1-3 km layer. The latter is likely associated with dust aerosols, which absorb solar radiation.

Rainfall arrives at the end of April and increases regularly to reach 3 *mm. day*$^{-1}$ in June (Fig. 9j). During this period, the ITCZ is just south of 15°N so that there is a net cooling/moistening in the low levels (Fig. 9a,b), which is mostly explained by the arrival of the monsoon flow in the lowest 1 km (Fig. 9g, h). The relevant processes are consistent with the previous analysis: turbulent fluxes and shallow convection keep on warming the low levels (Fig. 9c,d), while the return flow of the SMC clearly appears with a warming/drying between 1,5 km and 3 km. Rainfall rapidly reaches its maximum (5 *mm. day*$^{-1}$) in August, when the monsoon is fully developed with deep convective heating/ drying in the free troposphere (Fig. 9a, b) compensated by ascent (Fig. 9g, h). Consistent with Figures 7 and 8, the net tendency of the budgets is a warming/drying in the low levels, associated with the retreat of the monsoon flow (Fig. 9a,b ; Fig. 9g,h).

In summary, the vertically integrated budget of θ and q in June is considered, when all the key mechanisms are already at play (Fig .10). There is a net warming of the SHL by turbulence over the region from 20°N-30°N, while warming by deep convection is balanced by advection and radiative cooling (Fig. 10a). The northern Sahel (10-20°N) shows a net moistening (Figs 6,9,10) with a dramatic increase just south of the SHL (Fig. 10b). At this time, the advection by the monsoon flow is the leading moistening process over the northern Sahel (15°-20°N), while surface evaporation is more significant to the south, where rainfall feeds the ground hydrology. Note that the net effect of E-P is a drying over the continent. This view of the budgets highlights the key role of dry processes with surface sensible fluxes increasing the large scale temperature gradient between the SHL and Guinean Coast. The moistening of the southern flank of the SHL is thus favoured with an increase of the

moistening by the monsoon flow while surface evaporation feeds the atmosphere with moisture. As shown with the analysis of the vertical structure of the budget (Fig. 6-9), the vertical transport of moisture is accomplished by the turbulent eddy fluxes and shallow convection in the 1.5–3 km layer.

Here it is argued that this mechanism is acting during the whole seasonal cycle around the ITCZ so that the seasonal cycle of the ITCZ may be viewed as a translation of this picture which is modulated by the evolution of surface conditions (cold tongue, vegetation and surface albedo notably). As already pointed out by Thorncroft et al. (2011), the advection by the SMC is key to build a maximum in the convergence of the moisture flux at 850 hPa north of the ITCZ. It is also in good agreement with the mechanism shown by Hagos and Cook (2007) and Tomas et al. (1999) with inertial instability occurring all along the season favouring convection just north of the $\eta=0$ contour. However, we go further into the process analysis to determine how the moist and dry processes can combine to cause the humidification. The turbulent eddy fluxes added to the ground evaporation – the boundary condition for turbulence - appear to be of prime importance in the timing of the monsoon arrival at a particular latitude while convective downdrafts decrease (increase) humidity (temperature) within the ITCZ. This underscores the overall role of moisture transport, water phase changes and water recycling on the monsoon. Their relative contributions to the summer monsoon regime are explored in the next section using sensitivity experiments.

## 5. Sensitivity to key processes

The sensitivity experiments are started at the end of the second year of the REF experiment and integrated for during 1 year using the forcing from the REF experiment. Sensitivity experiments with longer integration periods show little variations so that the

results presented herein were found to be not very sensitive to the initialization. Continental averages of θ and θe in the 0-500 m layer as well as the maximum streamfunction in the ITCZ and in the SMC are analyzed.

a) Impact of convective downdraft and precipitation efficiency

The previous section supports the idea that the intensity of convective downdraft which is driven by the precipitation efficiency, Preff, has an significant impact on the monsoon regime. On a conceptual sense, one expect Preff to be low in a dry environment, reaching zero over the desert, and higher values in a wetter environment typical of the Guinean region. There is however no clear quantitative agreement on how Preff varies with the environmental properties like wind shear, relative humidity or with the stage of convection (Ferrier et al. 1996, Gao 2004) which makes it a parameter which is difficult to constrain in convective parameterisation. The role of downdrafts is thus explored in the 2D in a simplified bulk approach by fixing Preff to a constant value - regardless of the latitude or the environmental properties – between Preff=0 (all rainfall evaporates) and Preff=1 (all rainfall reaches the surface) in the convective scheme. Note that the horizontal-averaged value of Preff in the REF experiment is ~0.8 (Fig. 11, left, dashed vertical line).

The 2D model exhibits a transition from a rainfall peak over the Guinean coast and a reduced rain band extension for a weak Preff (~0.0-0.2), to a more intense Sahelian rainfall peak (7 mm $d^{-1}$) and a more northerly placement of the rain band for a high Preff (~0.90-1.00). A double rainfall peak is found for intermediate values of Preff. At the continental scale, a lower Preff leads to a linear decrease of both rainfall and θe, together with an increase in θ (Fig.s 11b, 13a).

The sensitivity to downdrafts is somewhat counterintuitive regarding the previous budget analysis since one might expect a suppressed downdraft to dry/warm the atmosphere and

block the monsoon. Here, the two most extreme regimes for Preff (0 and 1) are considered in more detail compared to the REF experiment. Consistent with Fig. 11, removing downdrafts (Preff=1) leads to a northward shift of the rain band with a more moist and cool atmosphere (Fig. 12a). This leads to enhanced surface latent heat fluxes (owing to the increased rainfall) and weaker sensible heat fluxes. When only resolved precipitation can reach the ground (i.e. Preff=0), the opposite pattern is found with reduced θe and higher θ associated with stronger sensible heat fluxes compensating the loss of latent heat flux (Fig .12c).

In summary, the precipitation efficiency of deep convection modulates the rainfall amount reaching the ground such that higher Preff leads to a broader and more intense rain band. The final sensitivity is related to the link with ground hydrology, i.e. the water recycling, which allows the convective rainfall to feed-back on the WAM. The latter process is investigated in the next subsection.

b) Impact of water recycling

In this set of experiments, the 2D model is modified to modulate the water recycling. Land surface models used in regional and global climate models typically use sub-grid parameterizations for surface runoff and canopy interception, but both the implementations and the parameter values which characterize the sub-grid distributions of these processes vary greatly among models and can lead to a large amount of uncertainty (defined as inter-model spread). These parameterizations can potentially exert strong controls on the Bowen ratio (especially in water limited regions, such as the Sahel) and the actual amount of soil water which can be recycled with the atmosphere. Thus, a simple first order approach is used to explore the impact of the maximum possible range of surface responses to rainfall on the recycling.

Assuming that the soil water storage change is relatively small (compared to the other budget terms) when averaged over the period JAS, the water balance is given in the REF experiment by P = E + L, where E stands for surface evaporation, P, for surface precipitation and L for the loss by runoff (mainly) or drainage. Therfore, the forcing mechanism is the amount of precipitation reaching the ground. In the $K_{RCL}$ experiments, the water balance has been modified following equation (4),

$$K_{RCL}P = E + L + \underbrace{(K_{RCL} - 1)P}_{L^*}; \; with \; 0 \le K_{RCL} \le 1 \quad (4)$$

In that balance the fraction (1- $K_{RCL}$) of precipitation is removed from the system before it reaches the ground so that the forcing of evaporation is $K_{RCL}$ P only, instead of P. For budget purpose, the fraction (1- $K_{RCL}$) is counted as a supplementary artificial runoff, L*, but the effective forcing of the ground hydrology is given by $K_{RCL}$P, ensuring the surface evaporation decreases with $K_{RCL}$.

On a first order, the ground evaporation is modulated by $K_{RCL}$ ranging from its REF value ($K_{RCL}$ =1), down to E=0 for $K_{RCL}$ =0. In the latter case, all of the precipitation is converted into runoff $L^*$ leading to a significant removal of water from the system and thus a drying of the atmosphere for the new equilibrium state. The obtained rainfall distribution is relatively steady with a persistent Sahelian peak of rainfall at 12°N characterized by a decrease of rainfall intensities for low $K_{RCL}$ and an overall reduction of the rain band extent (Fig. 11d,e). A single peak of precipitation is obtained when $K_{RCL}$ is reduced ($K_{RCL}$ <0.7) associated with higher θ and lower θe.

Regarding the extreme case where no water recycling is allowed**,** the reduction of rainfall is obtained with a warming/drying consistent with the enhancement of the surface sensible heat flux which compensates for the loss of latent heat flux (Fig. 13a,b), somewhat like the Preff=0 experiment. In this case, the circulation is driven by the sensible heat flux

which reinforces the SMC (Fig. 11f) and hence increases the moisture convergence over the Sahel. The ITCZ streamfunction is also strengthened, but the reasons for that need further investigation although it may be linked to the transition from a double to a single peak precipitation peak

A key result is that the water recycling plays a major role in terms of feeding the atmosphere with moisture, implying a variation of ~ 20-30% for the summer season precipitation for the full range of $K_{RCL}$. It also modulates the northward extent of the rain band so that if the ocean were the only source of moisture, the rain band would not penetrate as far to the north.

The role of ground-atmosphere coupling may, however, depend on the numerical model considered. As an example the evaporative fraction, defined by the ratio of evaporation by the precipitation, obtained from an ensemble of land surface models forced by satellite based rainfall from ALMIP[2] (Boone *et al.* 2010), shows a typical inter-model variation of 0.2-0.3, with a multi-model average value from 0.4 at the Guinean Coast to 0.8-0.9 in the Sahel (Fig. 14). Such variations may modulate the rainfall amounts, cause the rainfall spatial distribution to have a single or double peak, and may also change the response of the WAM to precipitation efficiency. The importance of the influence of land surface hydrology on surface fluxes in coupled systems has been known for some time, but in this experiment we have attempted to explore this effect specifically for the WAM and compared to other key sensitivities, such as the precipitation efficiency from the previous section. This simple sensitivity test also avoids issues related to the prescribed vegetation distribution, and the specifics related to the canopy interception parameterizations and the sub-grid surface runoff scheme, which can all influence the evaporative fraction: the goal here is to study a simple first order effect on water recycling. A message of this paper is that there is a need to evaluate

2 AMMA Land SurfaceModel Intercomparison Project, http://www.cnrm.meteo.fr/amma-moana/amma_surf/almip/present.html

and better understand the evaporative fraction in climate models and its dependence upon the rain rate and surface processes in order to obtain a signature of the model dependency in the light of the strong sensitivity of the WAM to the recycling. Finally, note that the effect of surface evaporation being mitigated by the reinforcement of the SMC might be somewhat overactive here since the 2D model tends to overestimate the strength of the SMC circulation (see section 2c). The next series of experiments thus explores the sensitivity of the WAM to the SMC transport.

c) Impact of the SMC

As shown in the budget analysis in section 4, the advection by the SMC is critical for building the moisture convergence along the northern edge of the ITCZ. The meridional circulation can be modulated during the season by intra-seasonal events, for example African Easterly waves (AEW, Poan et al. 2014) modulate the advection ahead of and behind the AEW trough. Stronger or more frequent AEWs may thus alter the mean magnitude of the SMC. Since the SMC is driven by the surface sensible heat flux meridional profile (Hagos and Zhang 2009) , changes in strength of the SMC may also occur depending on the surface features such as surface albedo (which controls the total enthalpy flux) or vegetation growth (which mainly impacts the Bowen ratio).

In this series of sensitivity experiments, the impact of variations in the intensity of the transport of moisture and temperature by the SMC is investigated. The SMC is first defined as the continental latitude where the meridional wind is southerly at 925hPa and northerly at 700 hPa. In a series of experiments, the corresponding meridional advections of $\theta$ and q are modulated by a coefficient $K_{SMC}$=0,0.1,0.2,…0.9,1 within the SMC region (Fig. 11 right column). This is done directly in the model's prognostic equations of $\theta$ and qby removing a

part (1- $K_{SMC}$) of the meridional advection terms using a stable finite differential upstream scheme. It thus leaves active only a $K_{SMC}$ part of the meridional advection in the simulation.

The weakening of the SMC advection shows the most dramatic change among the processes investigated in this study, with a southward shift of both the northern margin and the peak rainfall (Fig. 11g) corresponding to a drying of the continent (Fig. 11h) for all values of $K_{SMC}$. The reduction of the advection by the SMC mainly dries the continent and leads to higher rainfall in the range $0.2 < K_{SMC} < 0.7$ (Fig. 11h) associated with a stronger maximum of the ITCZ circulation (Fig. 11i). For the extreme limit for which no advection is allowed within the SMC ($K_{SMC}=0$), the southward shift of the rain band and the continental drying are found as before, but precipitation is reduced (Fig. 11h, 15a).

The effect of the monsoon flow (0-1.5 km) can be separated from the return flow (1.5-3 km) by setting the temperature and moisture advection to zero in each layer separately compared to the $K_{SMC}=0$ experiment. The result indicates that the humidification by the monsoon flow is the leading process within the SMC (Fig. 15b), and that the return flow, which is far less significant than the monsoon flow, contributes to blocking the monsoon penetration (Fig .15c). These experiments confirm the key role played by the SMC in moistening the continent and helping the monsoon move towards the Sahel (which is consistent with Thorncroft *et al*, 2011) Since intraseasonal events may modulate the SMC, it is suggested here that they cause a possible interaction between the large-scale circulation (larger than regional) and the WAM.

## 6. Discussion and conclusions

In this study, an idealized framework to study the WAM annual cycle is presented. Starting from the axisymetric model developed by PL07, a new methodology is proposed to derive the forcing of temperature and humidity, consisting in relaxing the temperature and

humidity toward the monthly mean fields of a reanalysis in a first step, and then using those tendencies as prescribed forcings in a second simulation. The 2D framework can then produce a more realistic mean annual cycle with the main features consistent with those observed.

The main mechanisms responsible for the annual movement of the ITCZ over land are then examined, and the importance of the role of the lowest 3 km of the atmosphere is highlighted. Consistent with Hagos and Cook (2007) and Thorncroft *et al*. (2011), a slowly-evolving large scale environment drives the seasonal migration of the rain band, associated with moisture convergence to the north of the ITCZ at 925 hPa, and within the ITCZ at 850 hPa, together with a warming of the SHL by turbulence and radiation. The region is also inertially unstable, favouring wind convergence in the low levels. The present study supports the idea that these mechanisms are at play during the whole annual cycle, resulting in a translation of this structure.

The budget analysis and sensitivity experiments allow an identification and ranking (in terms of importance) of the key process which shape the monsoon annual cycle. The advection by the shallow meridional circulation (SMC) between the rain band and the Sahara is a 1$^{st}$ order process in the determination of the location and extent of the WAM rain band. Variations in the SMC intensity may occur in response to intraseasonal events (Poan et al. 2014) or to the variation in the surface sensible heat flux (Hagos and Zhang 2009). Using highly idealized experiments modulating directly the transport of temperature and humidity within theSMC, it is shown that a weaker SMC leads to a more southerly location of the rainfall maximum and a reduced latitudinal extension of the rain band mainly owing to the monsoon flow, which advects moisture ahead of the ITCZ. The return flow is a second order process compared to the monsoon flow advection: it has the opposite effect which is associated with a more inland penetration of the rain band (when the return flow is removed).

Our results also show that when sufficient moisture is advected by the large scale meridional circulation causing deep convection to develop over land, the processes controlling the amount of precipitation, such as convective downdrafts, and those modulating the response of the surface, such as ground evaporation and water recycling, appear to play a significant role in shaping the seasonal cycle and overall rainfall spatial pattern.

More efficient deep convection (defined here as more rainfall reaching the surface owing to less evaporation in the atmosphere) results in more surface evaporation which ultimately moistens the atmosphere and reinforces the monsoon northward migration. Therefore the water recycling is the pathway which allows the WAM to respond to a change in the precipitation efficiency of deep convection. It is effective thanks to the long response timescale of ground evaporation to previous rainfall, in the range of 1-70 days (Lohou et al. 2013) compared to the one of atmospheric diffusive processes that damp the effect of downdraft evaporation within a time of ~1-3 hours. The leading effect is thus the increase of precipitation at the ground which modulates the surface evaporation. Considering the precipitation efficiency, it is physically modulated by the environmental humidity, which is also modulated by the large-scale subsidence prevailing over the Sahel. It is proposed that a possible way in which the large-scale circulation acts on the WAM might thus be through the modulation of environmental humidity and hence the precipitation efficiency.

Overall, West Africa appears as a region where the surface-atmosphere coupling plays a significant role in the regional climate, as pointed by out by Koster *et al*. (2004) using an ensemble of GCM models. The Sahel also stands out as an area with significant soil moisture-atmosphere coupling using surface reanalysis products (Dirmeyer 2011). Finally, there is a need to improve the understanding of coupling using observations (Dirmeyer et al. 2009), and such efforts are ongoing. Such studies should ultimately help improve the representation of coupling in GCMs.

An original aspect of this study is that we present a qualitative ranking of the different contributions to the summer rainfall season with the 1st order process being identified as the large-scale advection. The water recycling is then key for providing the atmosphere with moisture during the summer when SSTs over the Gulf of Guinea are colder than in spring. Once convection is active, convective downdrafts modulate the amount of rainfall reaching the ground and thus the feedback with the atmosphere.

The metrics proposed with the sensitivity experiments offer a synthetic view of the behaviour of the 2D model. It is argued here that these types of sensitivity experiments, which exhibit responses in the same range as those obtained with current climate models (Roehrig et al. 2013), could form the basis for a useful test-bed in order to get more insight into GCM general behaviour. In particular, this study stresses the need for a better understanding and modelling of the processes associated with precipitation efficiency, ranging from entrainment/detrainment (Oueslati and Bellon 2011 for example) to the interaction with large-scale vertical velocity, and those associated with ground-atmosphere water fluxes over West Africa (Boone et al., 2010 for example). The results are obtained here using a particular set of parameterizations so they need to be confirmed using other numerical models, and eventually ideally with a high resolution model. Finally, the processes analyzed here result from a strong coupling with other processes within the WAM that are not addressed here, such as cloud–radiation interactions or ocean-atmosphere coupling, which could be further investigated in future studies using the model framework presented herein.

## REFERENCES

Bechtold, P., E. Bazile, F. Guichard, P. Mascart and E. Richard, 2001: A mass flux convection scheme for regional and global models. Quart. J. Roy. Meteor. Soc., 127, 869-886.

Biasutti M., A. H. Sobel, and S.J. Camargo, 2009. The role of the Sahara Low in summertime Sahel rainfall variability and change in the CMIP3 models. Journal of Climate: 22:5755-5771. doi:10.1175/2009JCLI2969.1

Boone, A., and CoAuthors, 2009: The AMMA Land Surface Model Intercomparison Project. Bull. Amer. Meteor. Soc., 90(12), 1865-1880, doi:10.1175/2009BAMS2786.1

Boone, A., Y. Xue, I. Poccard-Leclerq, J. Feng, and P. deRosnay, 2010: Evaluation of the WAMME model surface fluxes using results from the AMMA land-surface model intercomparison project. Clim. Dynamics, 35(1), 127-142. DOI 10.1007/s00382-009-0653-1

Bordoni S., and Schneider T., 2010: Regime Transitions of Steady and Time-Dependent Hadley Circulations: Comparison of Axisymmetric and Eddy-Permitting Simulations. J. Atmos. Sci., 67, 1643–1654. doi: http://dx.doi.org/10.1175/2009JAS3294.1

Charney, J. G., 1975: Dynamics of deserts and drought in Sahel. Quart. J. Roy. Meteor. Soc., 101, 193–202

Chong, M. and D. Hauser, 1989: A tropical squall line observed during the COPT81 experiment in West Africa PartII: Water Budget. Mon. Weather Rev. 117, 728-744, doi:10,1175/1520-0493(1989)117<0728:ATSLOD>2,0,CO;2

Chou , C., J. D. Neelin, and H. Su, 2001: Ocean-atmosphere-land feedbacks in an idealized monsoon. Quart. J. Roy. Meteor. Soc., 127, 1869–1891

Chou, C., and J. D. Neelin, 2003: Mechanisms limiting the northward extent of the northern summer monsoons over North America, Asia, and Africa. J. Climate, 16, 406–425

Cook K.H. and Vizy, EK, 2006: Coupled Model Simulations of the West African Monsoon System: Twentieth- and Twenty-First-Century Simulations. J. Climate, 19, 3681–3703. doi: http://dx.doi.org/10.1175/JCLI3814.1

Cook, K. H. (2015), Role of inertial instability in the West African monsoon jump, J. Geophys. Res. Atmos., 120, 3085–3102, doi:10.1002/2014JD022579.

Cuxart, J., Bougeault, Ph. and Redelsperger, J.L., 2000: A turbulence scheme allowing for mesoscale and large-eddy simulations. Q. J. R. Meteorol. Soc., 126, 1-30

Dee, D. P., and Coauthors, 2011a: The ERA-Interim reanalysis: Configuration and performance of the data assimilation system. Quart. J. Roy. Meteor. Soc., 137, 553–597, doi:10.1002/qj.828

Dirmeyer PA, Schlosser CA, Brubaker KL (2009) Precipitation, Recycling, and Land Memory: An Integrated Analysis. J Hydrometeor 10:278-288

Dirmeyer, PA (2011) The terrestrial segment of soil moisture-climate coupling. Geophys Res Let 38: L16702 DOI: 10.1029/2011GL048268

Eltahir, E. A. B., and C. L. Gong, 1996: Dynamics of wet and dry years in West Africa. J. Climate, 9, 1030–1042

Ferrier, B. S., J. Simpson, and W.-K. Tao, 1996: Factors responsible for precipitation efficiencies in midlatitude and tropical squall simulations. Mon. Wea. Rev., 124, 2100–2125.

Fouquart, Y., and B. Bonnel, 1980: Computations of solar heating of the earth's atmosphere: A new parametrization. Beitr. Phys. Atmosph., 53, 35-62

Gao, S., X. Cui, Y. Zhou, and X. Li, 2005: Surface rainfall processes as simulated in a cloud-resolving model. J. Geophys. Res., 110, D10202, doi:10.1029/2004JD005467.

Hagos SM, and Cook K.H., 2007: Dynamics of the West African Monsoon Jump. J. Climate, 20, 5264–5284. doi: http://dx.doi.org/10.1175/2007JCLI1533.1

Hagos SM, Zhang C. 2009. Diabatic heating, divergent circulation and moisture transport in the African monsoon system. Q. J. R. Meteorol. Soc. 136 (S1): 411 – 425.

Huffman, G.J., R.F. Adler, M. Morrissey, D.T. Bolvin, S. Curtis, R. Joyce, B McGavock, J. Susskind, 2001: Global Precipitation at One-Degree Daily Resolution from Multi-Satellite Observations. J. Hydrometeor., 2, 36-50.

Hurley J.V. and Boos W.R. , 2013: Interannual Variability of Monsoon Precipitation and Local Subcloud Equivalent Potential Temperature. J. Climate, 26, 9507–9527.
doi: http://dx.doi.org/10.1175/JCLI-D-12-00229.1

Janicot et Coauthors, 2011: Intraseasonal variability of the West African monsoon. Atmos. Sci. Lett., 12, 58–66, doi:10.1002/asl.280

Kalnay E, Kanamitsu M, Kistler R, Collins W, Deaven D, Gandin L, Iredell M, Saha S, White G, Woollen J, Zhu Y, Leetmaa A, Reynolds R, Chelliah M, Ebisuzaki W, Higgins W, Janowiak J, Mo KC, Ropelewski C, Wang J, Jenne R, Joseph D. 1996. The NCEP/NCAR
40-year reanalysis project. Bull. Am. Meteorol. Soc. 77 : 437 – 471

Koster and Coauthors, 2004: Science 20 August 2004: 1138-1140. [DOI:10.1126/science.1100217]

Lafore, J. P., J. Stein, N. Asencio, P. Bougeault, V. Ducrocq, J. Duron, C. Fischer, P. Hereil, P. Mascart, J. P. Pinty, J. L. Redelsperger, E. Richard, and J. Vila-Guerau de Arellano, 1998: The Meso-NH Atmospheric Simulation System. Part I: Adiabatic formulation and control simulations. Annales Geophysicae, 16, 90-109.

Lohou, F., L. Kergoat, F. Guichard, A. Boone, B. Cappelaere, J.-M. Cohard, J. Demarty , S. Galle, M. Grippa, C. Peugeot, D. Ramier, C. M. Taylor, and F. Timouk; 2013: Surface response to rain events throughout the West African monsoon. Atmos. Chem. Phys., 14, 3883–3898, 2014 doi:10.5194/acp-14-3883-2014

Maloney, E. D., and J. Shaman, 2008: Intraseasonal variability of the west African monsoon and Atlantic ITCZ. J. Climate, 21, 2898-2918.

Masson, V., J.-L. Champeaux, C. Chauvin, C. Meriguet, and R. Lacaze, 2003: A global database of land surface parameters at 1 km resolution for use in meteorological and climate models, J. Climate, 16, 1261-1282

V. Masson and CoAuthors, 2013: The SURFEXv7.2 land and ocean surface platform for coupled or offline simulation of earth surface variables and fluxes, Geosci. Model Dev., 6, 929-960

Mlawer, E.J., S.J. Taubman, P.D. Brown, M.J. Iacono, and S.A. CLough, 1997: Radiative transfer for inhomogeneous atmospheres: RRTM, a validated correlated-k model for the longwave. J. Geophys. Res., 102D, 16663-16682

Meynadier R, Bock O, Gervois S, Guichard F, Redelsperger J-L, Agusti-Panareda A, Beljaars A. 2010. West African monsoon water cycle. 2: Assessment of numerical weather prediction water budgets.J. Geophys.Res.115: D19107, DOI: 10.1029/2010JD013919

Nicholson, S. E. and P. J. Webster, 2007: A physical basis for the interannual variability of rainfall in the Sahel. Q. J. R. Meteorol. Soc. doi: 10.1002/qj.104

Noilhan, J., and S. Planton, 1989: A simple parameterization of land surface processes for meteorological models. Mon. Wea. Rev., 117, 536-549.

Okumura Y, Xie S-P., 2004 : Interaction of the Atlantic equatorial cold tongue and the African monsoon. J. Climate 17 : 3589 – 3602.

Peyrillé P, Lafore J.P., and Redelsperger J.L. , 2007: An idealized two-dimensional framework to study the west african monsoon. part i: validation and key controlling factors. J. Atmos. Sci., 64, 2765–2782. doi: http://dx.doi.org/10.1175/JAS3919.1

Oueslati, B., and G. Bellon, 2013 : Convective entrainment and large-scale organization of tropical precipitation : sensitivity of the CNRM-CM5 hierarchy of models, Journal of Climate, 26 (9), 2931-2946, doi:10.1175/JCLI-D-12-00314.1.

Pergaud, J., V. Masson, S. Malardel, and F. Couvreux, 2009: A parameterization of dry thermals and shallow cumuli for mesoscale numerical weather prediction, Bound.-Layer. Meteor., 132, 83-106

Pinty, J.-P. and P. Jabouille, 1998: A mixed-phase cloud parameterization for use in mesoscale non-hydrostatic model: simulations of a squall line and of orographic precipitations. Proc. Conf. of Cloud Physics, Everett, WA, USA, Amer. Meteor. soc., Aug. 1999, 217 – 220

Peyrillé, P., and J. P. Lafore, 2007: An idealized two-dimensional framework to study the West African monsoon. Part II: Large-scale advection and the diurnal cycle. J. Atmos. Sci., 64, 2783–2803, doi: http://dx.doi.org/10.1175/JAS4052.1

Philippon N., Mougin, E., Jarlan, L. and Frison P.L. (2005) Analysis of the linkages between rainfall and land surface conditions in the West Africa monsoon through CMAP, ERS-WSC and NOAA-AVHRR data, J. Geophys. Res. (Atmosphere), 110, D24115, doi:10.1029/2005JD006394. (plain text.pdf, 720K)

Poan E.D., Lafore, J.P., Roehrig R. and Couvreux, F., 2014 : Internal processes within the African Easterly Wave system. QJRMS, 141, 1121-1136. DOI: 10.1002/qj.2420

Ramel R., Gallée H., Messager C., 2006 : On the northward shift of the West African monsoon. Clim Dyn 26: 429–440. DOI 10.1007/s00382-005-0093-5.

Reynolds, R. W., N. A. Rayner, T. M. Smith, D. C. Stokes, and W. Wang, 2002: An improved in situ and satellite SST analysis for climate. J. Climate, 15, 1609–1625

R. Roehrig, F. Chauvin, and J.-P. Lafore, 2011: 10–25-Day Intraseasonal Variability of Convection over the Sahel: A Role of the Saharan Heat Low and Midlatitudes. J. Climate, 24, 5863–5878. doi: http://dx.doi.org/10.1175/2011JCLI3960.1

Roehrig R, Bouniol D, Guichard F, Hourdin F, and Redelsperger JL, 2013: The Present and Future of the West African Monsoon: A Process-Oriented Assessment of CMIP5 Simulations along the AMMA Transect. J. Climate, 26, 6471–6505. doi: http://dx.doi.org/10.1175/JCLI-D-12-00505.1

Schneider T., and Bordoni S., 2008: Eddy-Mediated Regime Transitions in the Seasonal Cycle of a Hadley Circulation and Implications for Monsoon Dynamics. J. Atmos. Sci., 65, 915–934.

Sultan and Janicot 2003: TheWest Africanmonsoon dynamics.Part II: The ‘‘preonset’’ and ‘onset’’ of the summer monsoon. J. Climate,16, 3407–3427

Tegen, I., P. Hollrig, M. Chin, I. Fung, D. Jacob, and J. Penner (1997), Contribution of different aerosol species to the global aerosol extinction optical thickness: Estimates from model results, J. Geophys. Res., 102, 23,895–23,915, doi:10.1029/97JD01864.

Thorncroft CD, Blackburn M. 1999. Maintenance of the African easterly jet. Q. J. R. Meteorol. Soc. 125 : 763 – 786

Thorncroft CD, Nguyen H, Zhang C, Peyrille P. 2011. Annual cycle of the West African monsoon: regional circulations and associated water vapour transport. Q. J. R. Meteorol. Soc. 137 : 129 – 147. DOI:10.1002/qj.728

Tomas, R. and P. J. Webster, 1997: The role of inertial instability in determining the location and strength of near-equatorial convection. Quar. J. Roy. Met. Soc., 123, 1445-1482

Tomas, R., J. R. Holton and P. J. Webster, 1999: The influence of cross-equatorial pressure gradient on the location of near-equatorial convection. Q. J. Roy. Meteor. Soc., 125, 1107-1127

Uppala SM and CoAuthors, 2005. The ERA-40 re-analysis. Q. J. R. Meteorol. Soc. 131 : 2961 – 3012

Vizy, E. K., K. H. Cook, J. Cretat, and N. Neupane, 2013: Projections of a wetter Sahel in the twenty-first century from global and regional models. J. Climate, 26, 4664– 4687.

Xue, Y. and J. Shukla, 1998: Model Simulation of the Influence of Global SST Anomalies on the Sahel Rainfall. J. Climate, 126, 2782-2792.

Zhang C, Nolan DS, Thorncroft CD, Nguyen H. 2008. Shallow meridional circulations in the tropical atmosphere. J. Climate, 21 : 3453 – 3470

Zheng X, Eltahir EAB, Emanuel KA. 1999. A mechanism relating tropical Atlantic spring sea surface temperature and West African rainfall. Q. J. R. Meteorol. Soc. 125 : 1129 – 1163.

**Table 1:** Summary of sensitivity experiments with their main characteristics. For the sensitivity experiments to downdraft, water recycling and transport by the SMC, the large-scale forcing is the same as in the REF experiment.

| **Process analysed** | **Description** | **Name** |
|---|---|---|
| **Large scale forcing** | Sensitivity to the forcing timescale $\tau_1$ | $\tau_1$=1,3,5 |
| **Downdraft** | Precipitation efficiency fixed to Preff | Preff=0,0.1,..0.9,1 |
| **Water recycling** | Ground infiltration modulated with $K_{RCL}$ | $K_{RCL}$=0,0.1,…,0.9,1 |
| **Transport of θ, q within the SMC** | Advection by the SMC modulated with $K_{SMC}$<br>No Advection within the 0-1.5 km layer<br>No Advection within the 1.5-3 km layer | $K_{SMC}$=0,0.1,…,0.9,1<br>0-1.5kmAdvOff<br>1.5-3kmAdv_Off |
| | | |

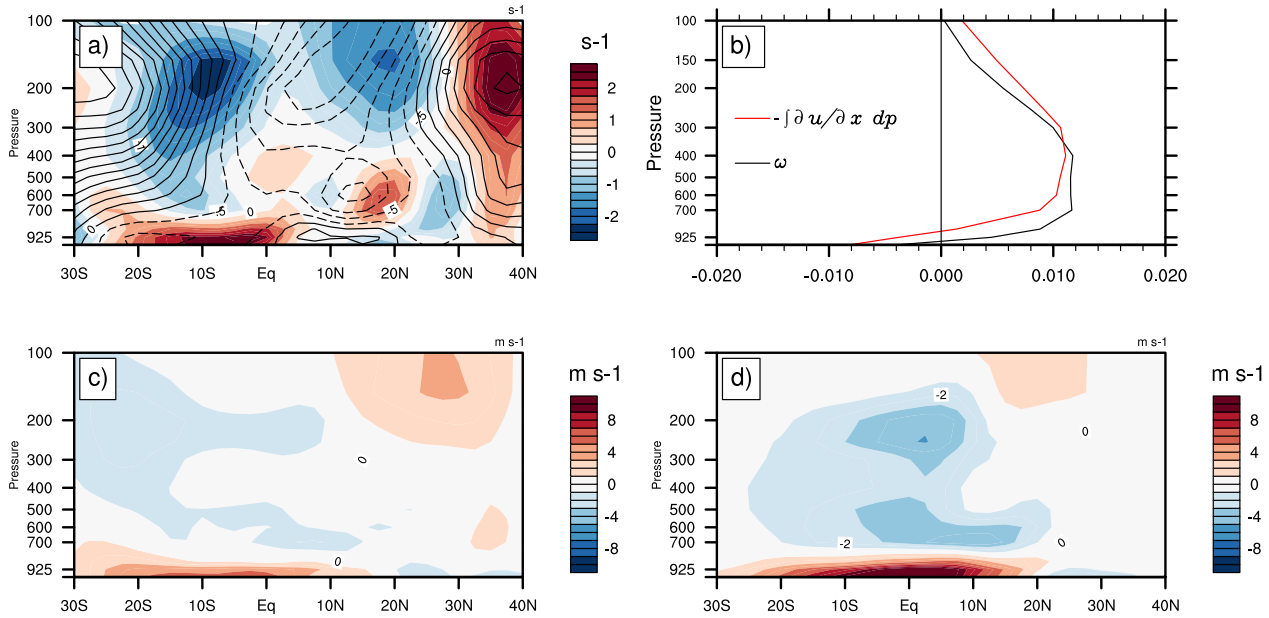


Figure 1: (a) JAS mean vertical cross-section of NCEP2 [10W-10E] mean zonal divergence (colour, $s^{-1}$) and zonal wind (contour, $m.s^{-1}$). (b) Vertical profile of [10W-10E]-[30S-40N] averaged pressure velocity (black) and pressure velocity obtained by integrating the [10W-10E] mean zonal divergence (red). (c) Same as (a) except for [10W-10E] mean meridional wind ($m.s^{-1}$, colours). (d) Same as (c) except for $V_{nd}$, the non-divergent meridional wind ($m.s^{-1}$) in the meridional-vertical plane. In (d) $V_{nd}$ is obtained after integrating over latitude $V_{nd} = \frac{1}{cos(\phi)} \int_{30S}^{40N} rcos(\phi) \frac{\partial \omega}{\partial p} d\phi$ where $\frac{\partial \omega}{\partial p}$ is the [10W-10E] mean vertical divergence (see text for details).

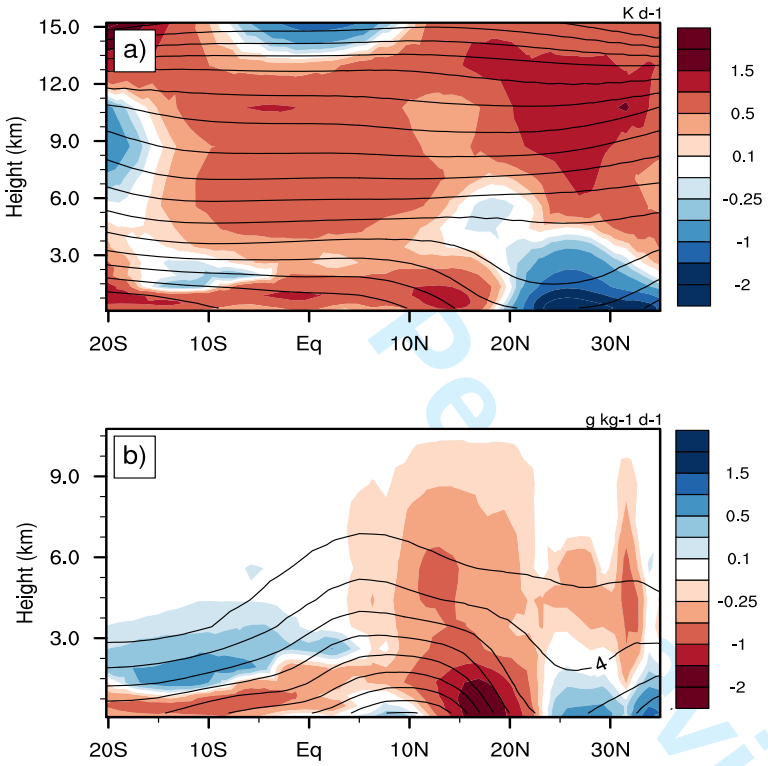


Figure 2: JAS mean forcing derived from a 3-day relaxation towards NCEP2 for (a) temperature ($K.d^{-1}$) and (b) humidity ($g.kg^{-1}.d^{-1}$), see text for details.

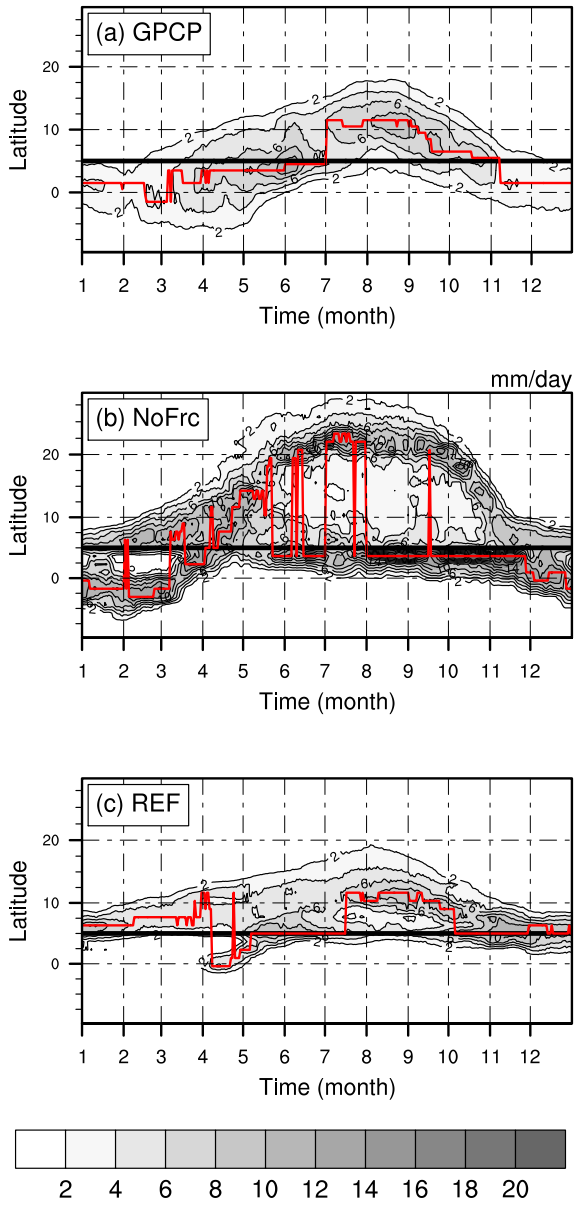


Figure 3: Time-latitude plot of daily rainfall ($mm.d^{-1}$) for (a) GPCP, (b) NoFrc experiment and (c) REF experiment. The red line indicates the ITCZ which is defined as the rainfall maximum in the current study.

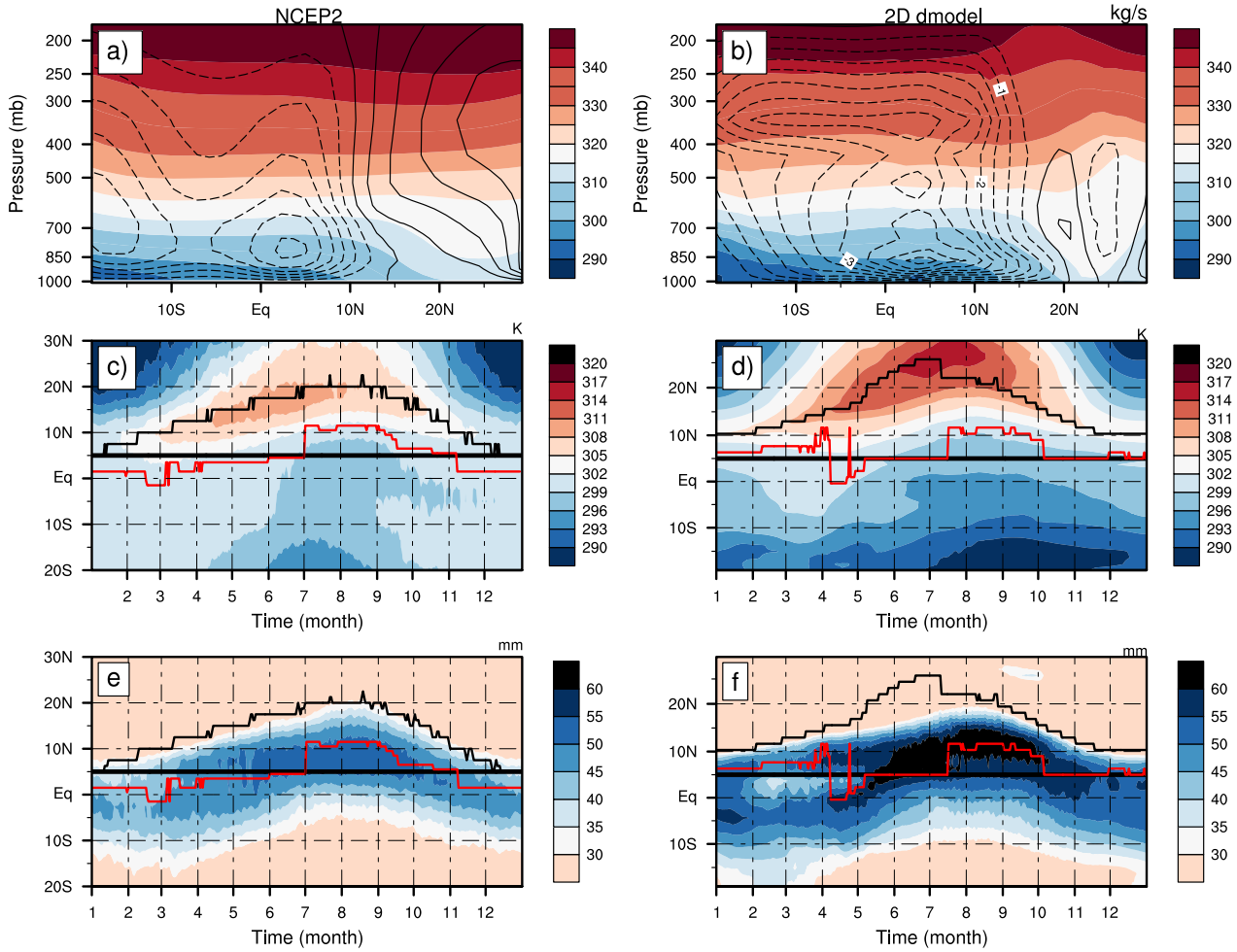


Figure 4: Upper panel: JAS mean meridional-vertical streamfunction (contour in $kg.s^{-1}$) and $\theta$ (colour, $K$) for (a) [10W-10E] zonal mean NCEP2 data and (b) the REF experiment. Middle panel: Time-latitude diagram of $[0-500m]$ averaged $\theta$ $(K)$ in (c) NCEP2 and (d) REF experiment. Lower panel: (e,f) same as (c,d) except for precipitable water $(mm)$. In (c,d,e,f), the red line depicts the ITCZ as the maximum rainfall and the black line represents the ITD $(v = 0)$.

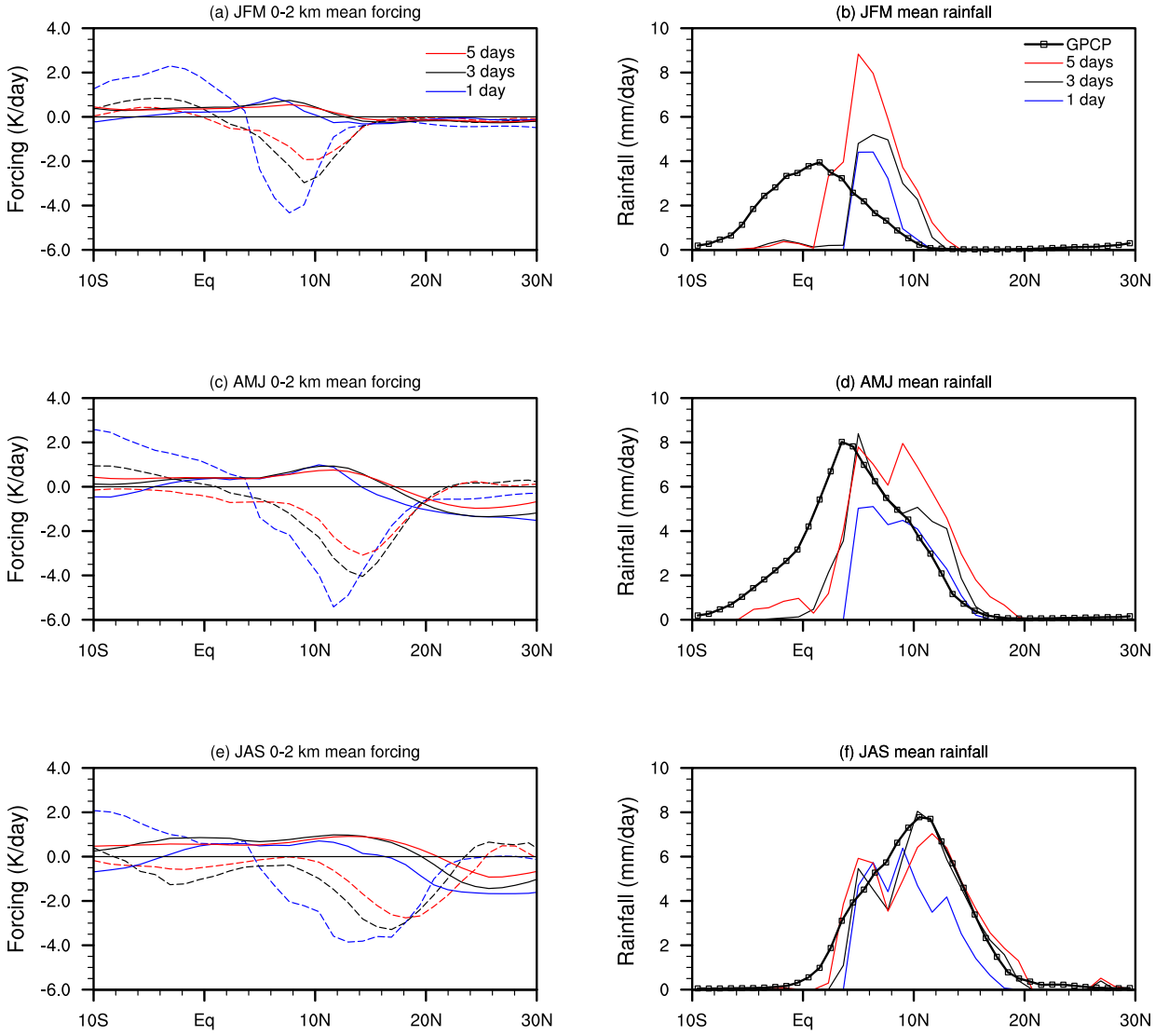


Figure 5: [0-2] km mean forcing of $\theta$ (solid, $K.d^{-1}$) and water vapour (dashed, $K.d^{-1}$) obtained with different relaxation timescales (left column), and the corresponding precipitation (right column, $mm.d^{-1}$) for (a,b) JFM , (c,d) AMJ and (e,f) JAS. In the right panel, the GPCP rainfall is added (square).

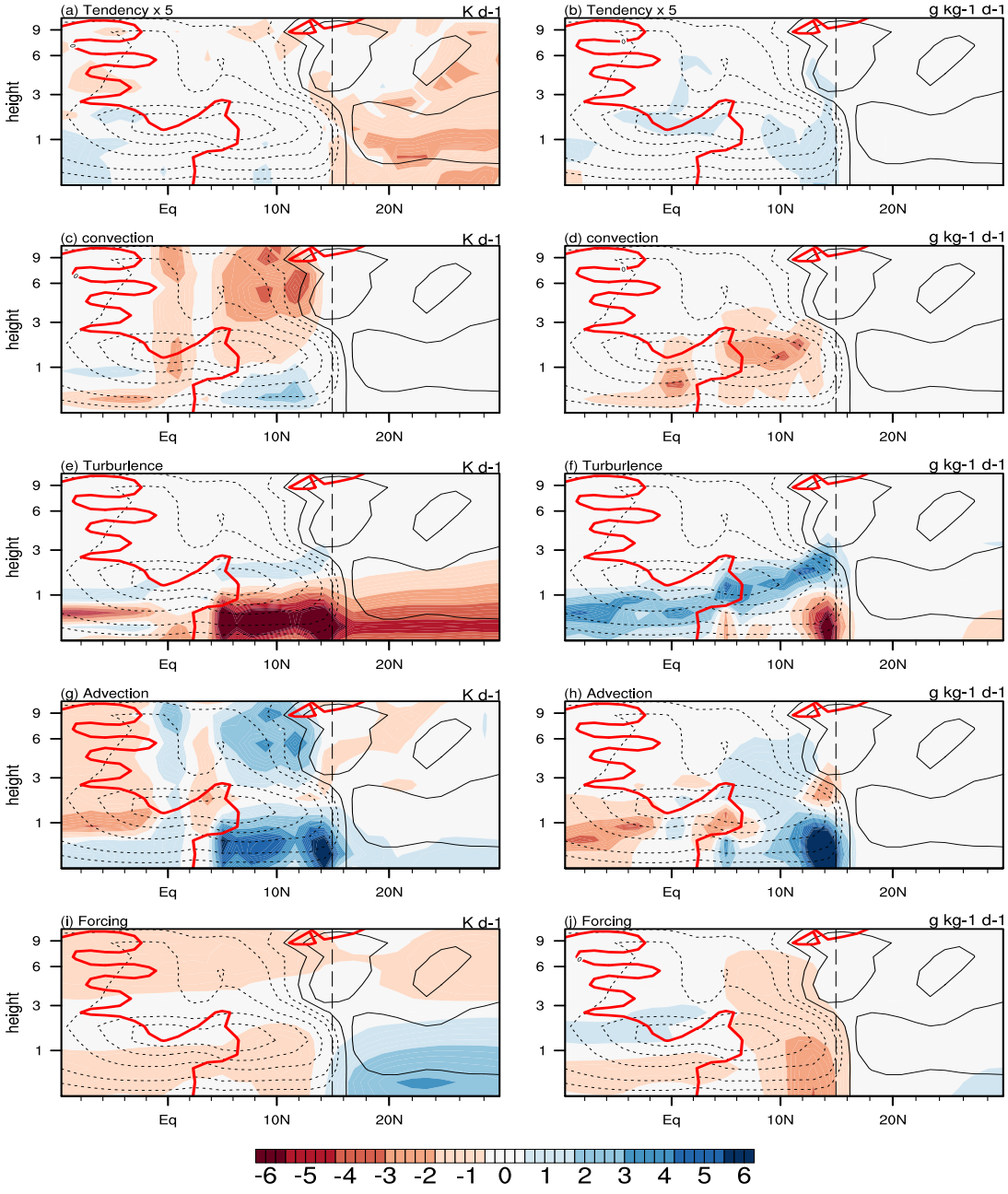


Figure 6: April mean meridional-vertical cross section of the streamfunction (contour, $10^{10} kg.s^{-1}$) superimposed on the different budget terms for $\theta$ (left column, in $K.d^{-1}$) and $q$ (left, in $g.kg^{-1}.d^{-1}$). (a,b) total tendency, (c,d) convection, (e,f) turbulence, (g,h) advection, (i,j) forcing. In (a,b), the total tendency is multiplied by 5. The red line denotes zero absolute vorticity ($\eta = \zeta + f$) with negative absolute vorticity to the left (south) of the line.

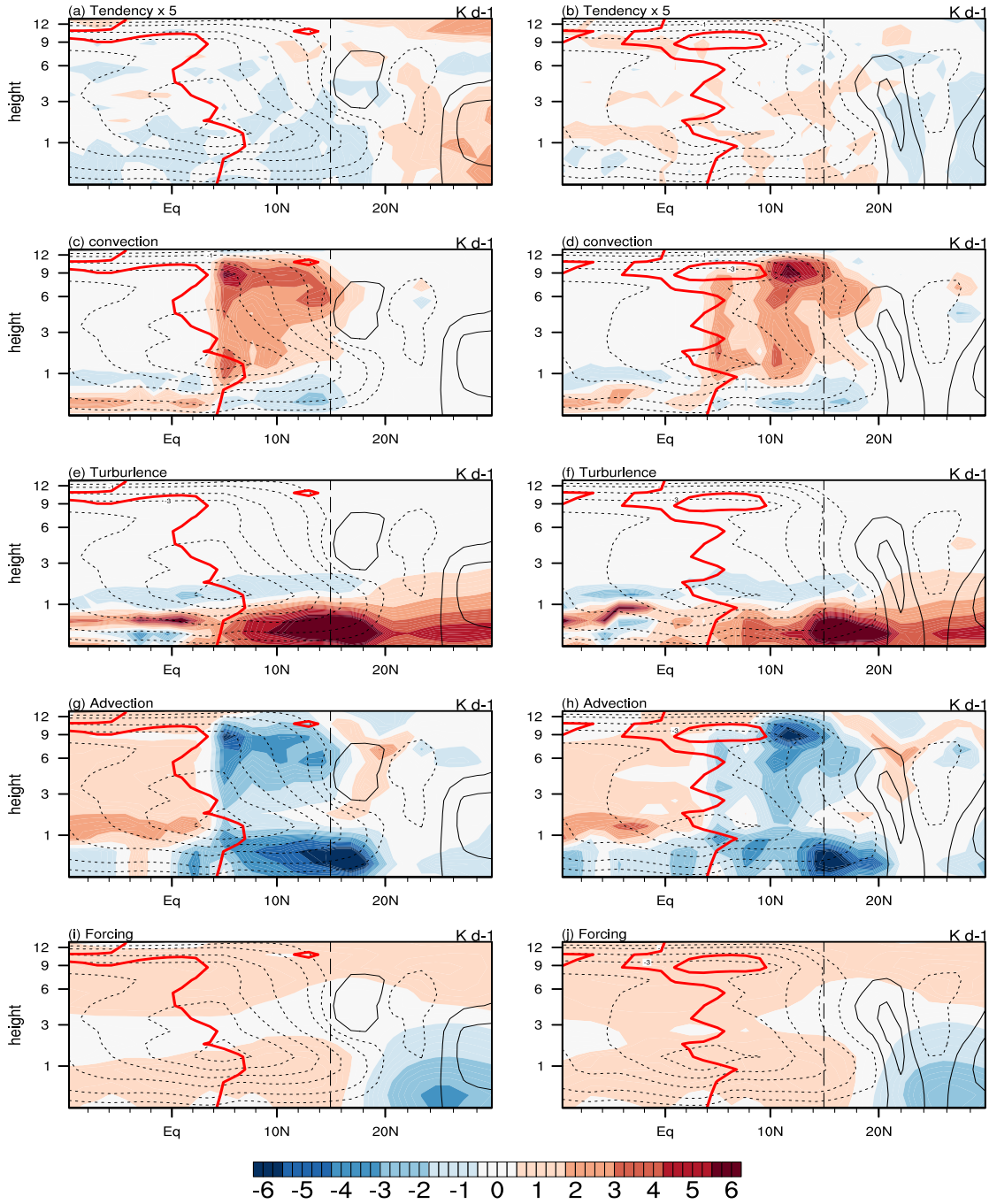


Figure 7: Latitude-height cross section of streamfunction (contour, $kg.s^{-1}$) superimposed on the $\theta$ budget ($K.d^{-1}$) in June (left column) and August (right column). (a,b) total tendency, (c,d) convection, (e,f) turbulence, (g,h) advection, (i,j) forcing. In (a,b) the total tendency is multiplied by 5. The red line denotes zero absolute vorticity ($\eta = \zeta + f$) with negative absolute vorticity to the left (south) of the line.

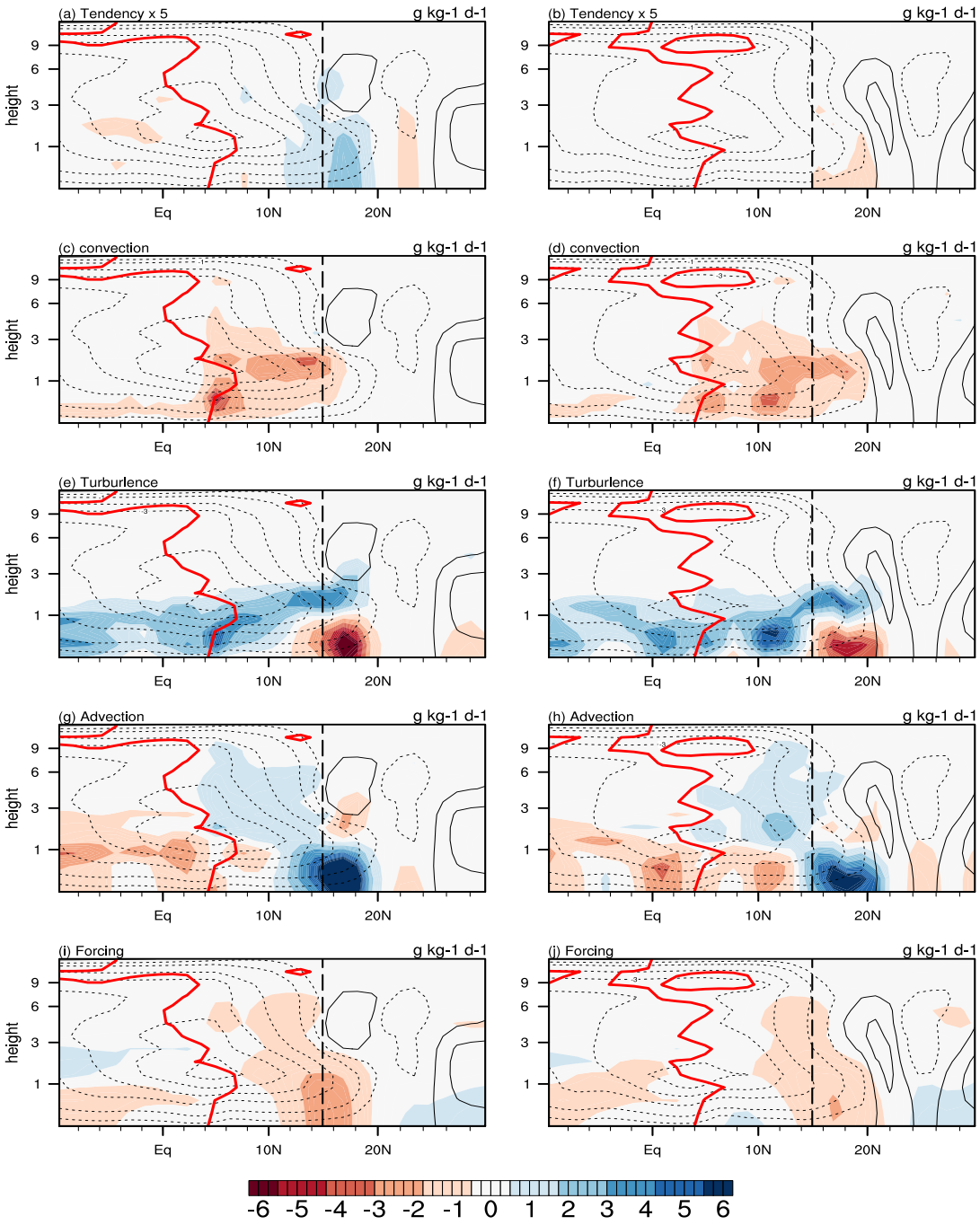


Figure 8: Same as Figure 7 except for humidity budget terms ($g.kg^{-1}.d^{-1}$).

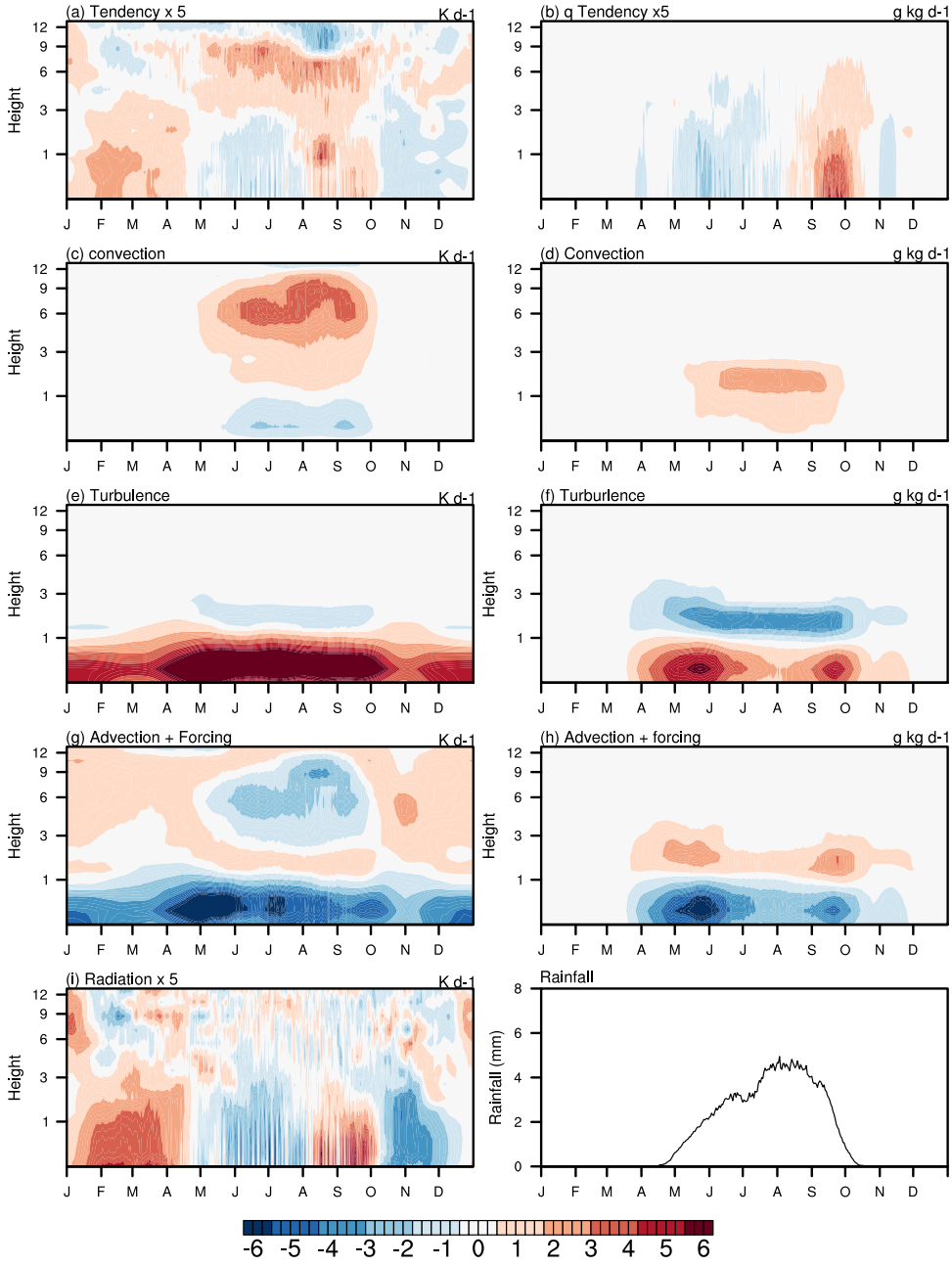


Figure 9: Left: Temporal evolution at latitude $15N$ in the REF experiment of the $\theta$ budget ($K.d^{-1}$): (a) total tendency, (c) convection, (e) turbulence, (g) advection + forcing, (i) radiation. Right: same as left except for humidity budget (($g.kg^{-1}.d^{-1}$): (b) total tendency, (d) convection, (f) turbulence, (h) advection + forcing and (f) precipitation ($mm.d^{-1}$). In (a,b,i), the total tendency term is multiplied by 5.

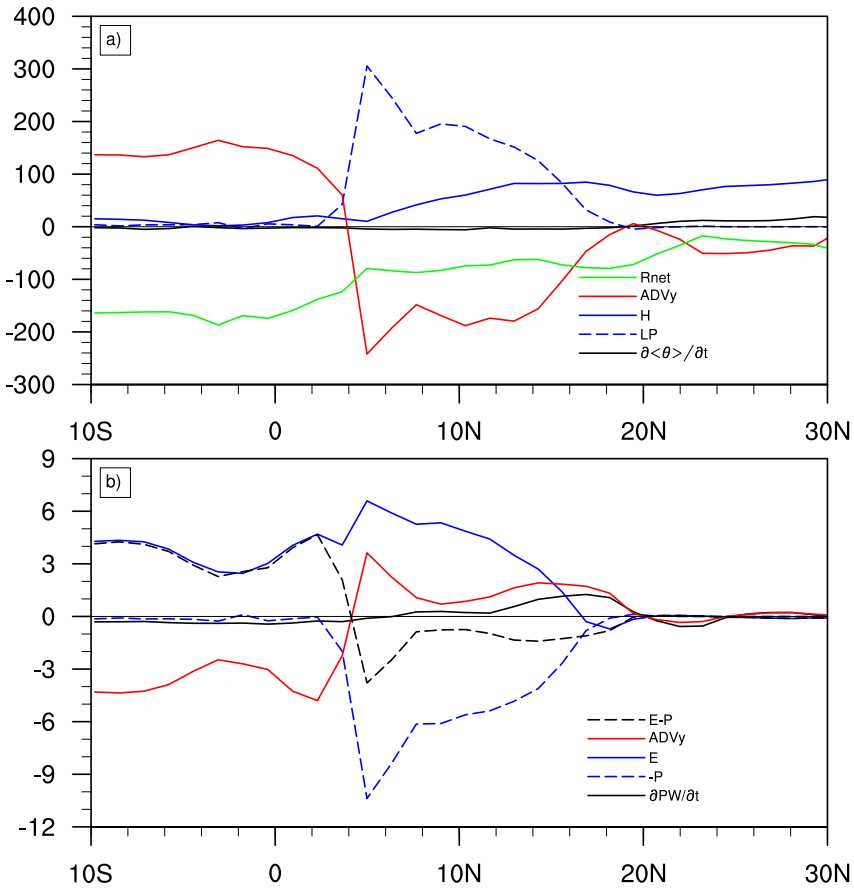


Figure 10: (a) June mean budget of column integrated $\theta$ ($W.m^{-2}$) given by $\frac{\partial <c_p \theta>}{\partial t} = R_{net} + Adv_y + H + LP$ where $R_{net}$ is the net radiation, $Adv_y$ is column integrated meridional advection, $H$ the sensible heat flux, $LP$ precipitation multiplied by the latent heat of vaporisation. (b) same as (a) except for the budget of PW ($mm.d^{-1}$) where $E$ stands for surface evaporation and $P$ is precipitation.

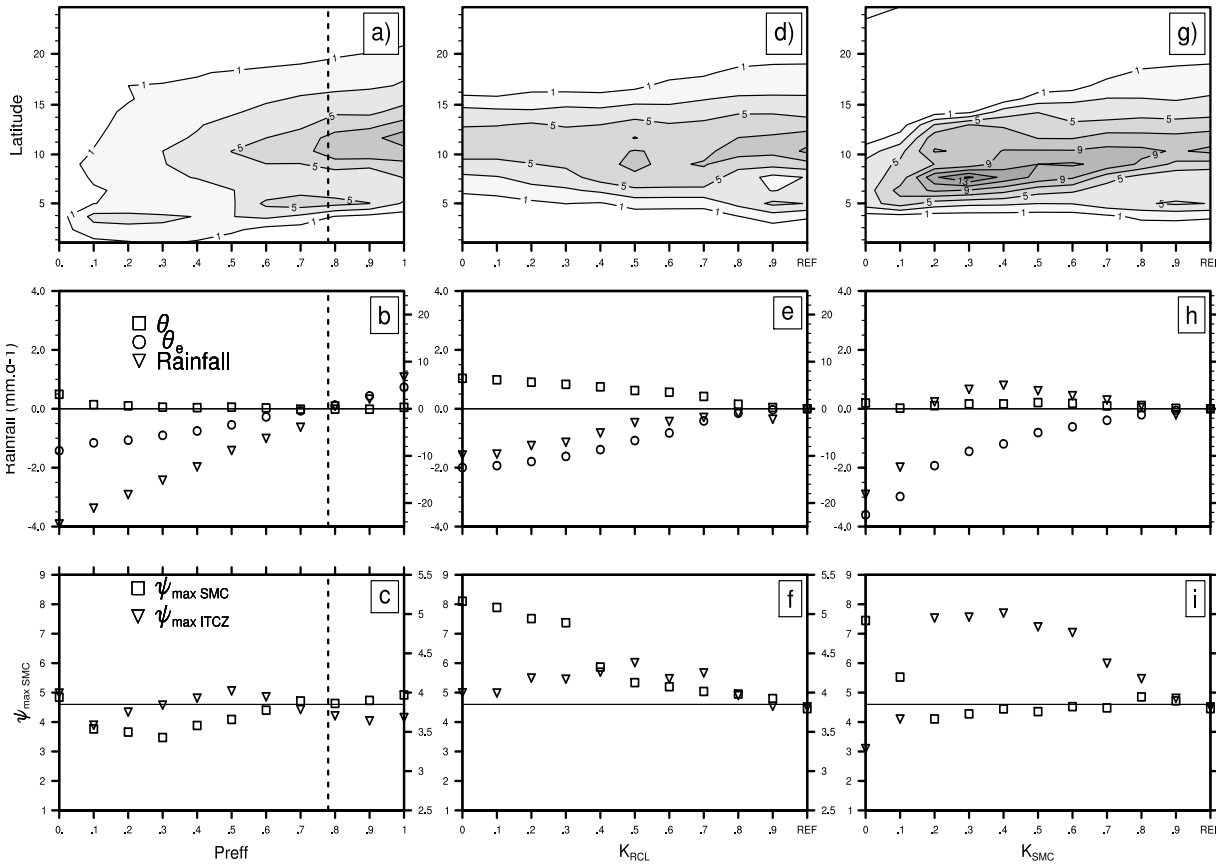


Figure 11: Left column: the JAS mean fields for the sensivity to downdrafts plotted against Preff for (a) the rainfall meridional distribution, (b) the averaged $[5N - 25N]$ departure from the REF experiment for rainfall (triangle), $0 - 500m$ averaged $\theta$ (square) and $0 - 500m$ averaged $\theta_e$ (circle) and c) the maximum magnitude of meridional streamfuntions,$\psi$, within the SMC (square) and within the ITCZ (triangle). Middle column: Same as left column except the plots show the sensivity to water recycling plotted against $K_{RCL}$. Right column: Same as left column except for results of the sensivity to the advection of $\theta, q$ within the SMC plotted against $K_{SMC}$. Units: Rainfall $mm.d^{-1}$, $\theta$ and $\theta_e$ in K, $\psi$ expressed as $10^{10}kg.s^{-1}$

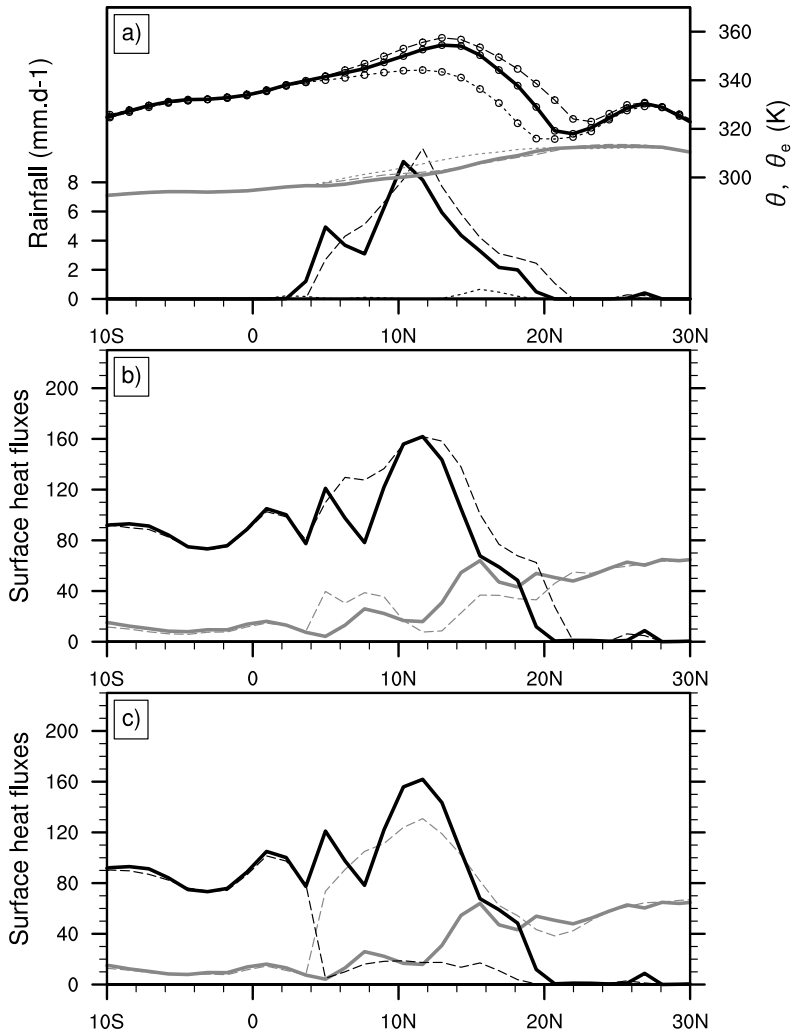


Figure 12: JAS mean meridional distribution from the REF experiment (solid), the Preff=0 (dotted) and Preff=1 experiment (dashed) for (a) rainfall (black, $mm.d^{-1}$), $0-500m$ averaged $\theta$ (gray, K) and $\theta_e$ (circle, K). (b) Surface sensible (gray, $W.m^{-2}$) and latent (black , $W.m^{-2}$) heat fluxes for the REF (solid) and the Preff=1 (dashed) experiments. (c) Same as (b) except for REF (solid) and Preff=0 (dashed) experiments.

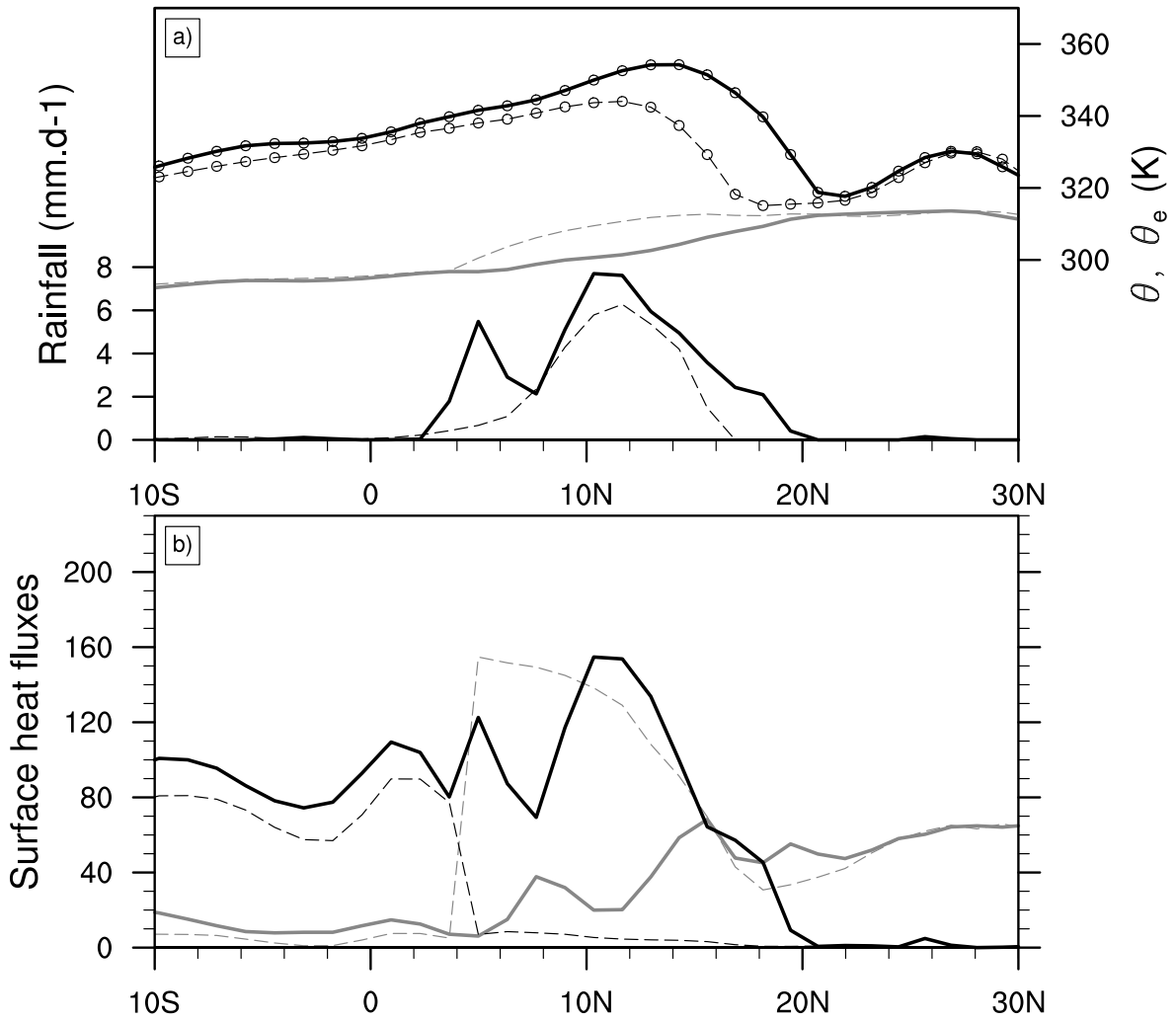


Figure 13: Same as Fig. 13 except for the REF (solid) and $K_{RCL} = 0$ (dashed) experiments.

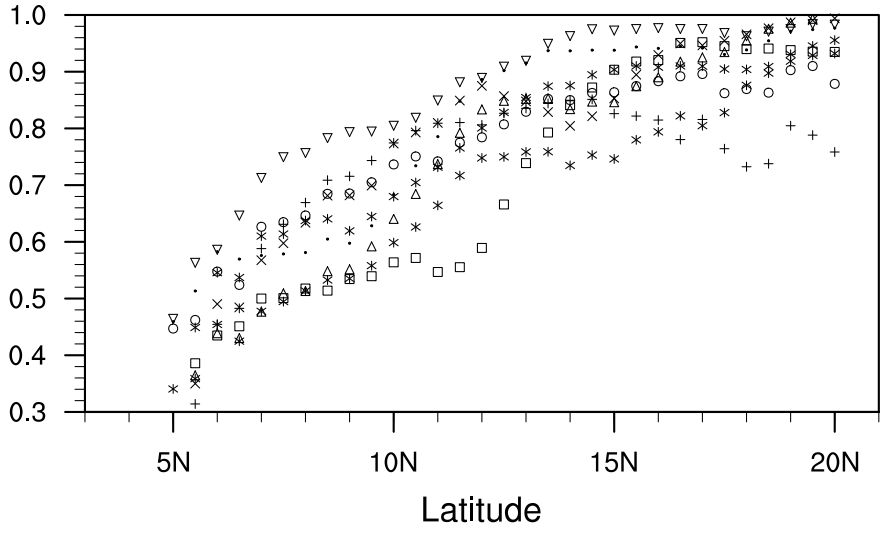


Figure 14: [10W-10E] mean evaporative fraction obtained from the ALMIP land surface models.

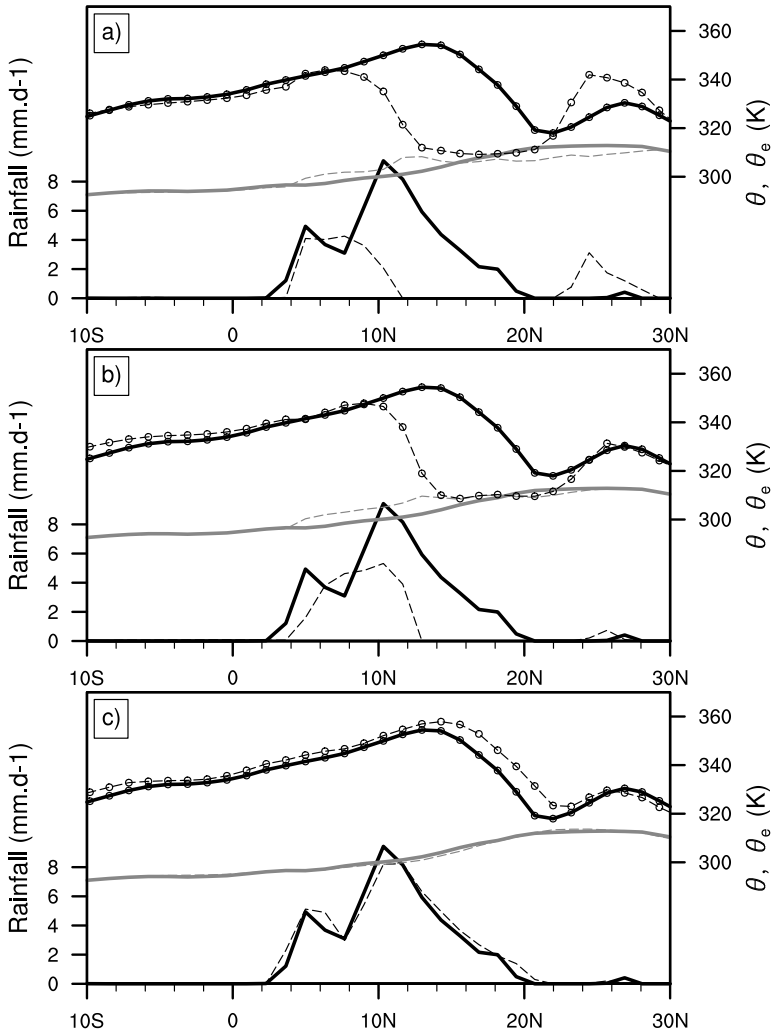


Figure 15: JAS mean meridional distribution of rainfall (black, $mm.d^{-1}$), $\theta$ (gray, K) and $\theta_e$ (circle, K) for (a) REF (solid) and NoSmcAdv (dashed) experiments. (b) Same as (a) except for the REF (solid) and 0-1.5kmAdvOff (dashed) experiments. (c) Same as (a) except for REF (solid) and 1.5-3kmAdvOff (dashed) experiments.